Expansion Dynamics in Fermionic Quantum Gases

Jussi Kajala

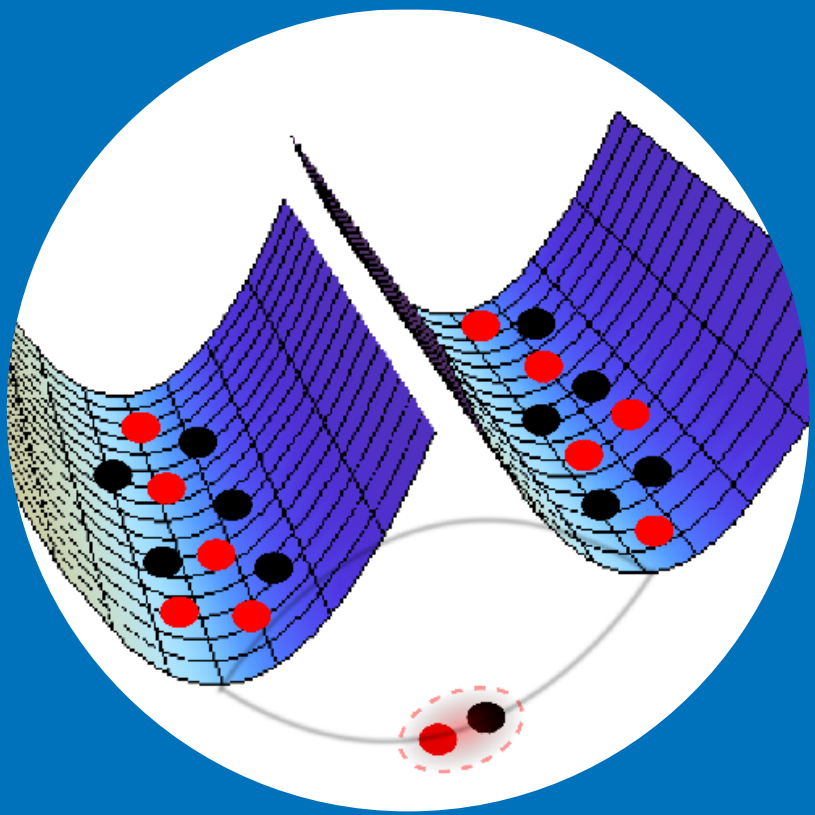

Aalto University

DOCTORAL DISSERTATIONS

Aalto University publication series
DOCTORAL DISSERTATIONS 120/2011

Expansion Dynamics in Fermionic Quantum Gases

Jussi Kajala

Doctoral dissertation for the degree of Doctor of Science in Technology to be presented with due permission of the School of Science for public examination and debate in Auditorium G at the main building of Aalto University School of Science (Espoo, Finland) on the 9th of December 2011 at noon.

Aalto University
School of Science
Department of Applied Physics
Quantum Dynamics

Supervisor
Prof. Päivi Törmä

Instructor
Prof. Päivi Törmä

Preliminary examiners
Prof. Robert van Leeuwen, University of Jyväskylä, Finland.
Prof. Kalle-Antti Suominen, University of Turku, Finland.

Opponent
Dr. Meera Parish, University of Cambridge, UK.

Aalto University publication series
DOCTORAL DISSERTATIONS 120/2011

ISBN 978-952-60-4372-2 (pdf)
ISBN 978-952-60-4371-5 (printed)
ISSN-L 1799-4934
ISSN 1799-4942 (pdf)
ISSN 1799-4934 (printed)

Unigrafia Oy
Helsinki 2011

Finland

The dissertation can be read at http://lib.tkk.fi/Diss/

Publication orders (printed book):
jussi.kajala@gmail.com

Aalto University

Abstract

Aalto University, P.O. Box 11000, FI-00076 Aalto www.aalto.fi

Author
Jussi Kajala

Name of the doctoral dissertation
Expansion Dynamics in Fermionic Quantum Gases

Publisher School of Science

Unit Department of Applied Physics

Series Aalto University publication series DOCTORAL DISSERTATIONS 120/2011

Field of research Ultracold Fermi gases

Manuscript submitted 20 September 2011 **Manuscript revised** 31 October 2011

Date of the defence 9 December 2011 **Language** English

☐ **Monograph** ☒ **Article dissertation (summary + original articles)**

Abstract

In this work we study dynamics of fermionic quantum gases. Radio frequency spectroscopy, Josephson oscillations, and time-of-flight dynamics are studied theoretically, and with the help of numerical simulations using the time-evolving block decimation algorithm.

The simulations of radio frequency spectroscopy shed light on the nature of excitations in a fermionic superfluid confined in a lattice. The Josephson oscillations in the presence of different potentials for up and down spins show that the asymmetric Josephson effect cannot be described by the traditionally established view of coherent tunnelling of Cooper pairs. The expansion dynamics of a band-insulating state reveals that we can explain the time development of two-component systems in a lattice using a simple two-site model. Finally, the time-of-flight expansion of an imbalanced superfluid restricted to move in one dimension provides a remarkably simple way for detecting the long-sought-for Fulde-Ferrell-Larkin-Ovchinnikov superfluid state.

Keywords Fermi gas, superfluidity, Fermi-Hubbard, TEBD, Kadanoff-Baym, superconductivity, cold gases, the Josephson effect, unitary dynamics, FFLO, collision dynamics.

ISBN (printed) 978-952-60-4371-5 **ISBN (pdf)** 978-952-60-4372-2

ISSN-L 1799-4934 **ISSN (printed)** 1799-4934 **ISSN (pdf)** 1799-4942

Location of publisher Espoo **Location of printing** Helsinki **Year** 2011

Pages 119 **The dissertation can be read at** http://lib.tkk.fi/Diss/

A? Aalto-yliopisto

Tiivistelmä

Aalto-yliopisto, PL 11000, 00076 Aalto www.aalto.fi

Tekijä
Jussi Kajala

Väitöskirjan nimi
Expansion Dynamics in Fermionic Quantum Gases

Julkaisija Perustieteiden korkeakoulu

Yksikkö Teknillisen fysiikan laitos

Sarja Aalto University publication series DOCTORAL DISSERTATIONS 120/2011

Tutkimusala Ultrakylmät fermikaasut

Käsikirjoituksen pvm 20.09.2011 **Korjatun käsikirjoituksen pvm** 31.10.2011

Väitöspäivä 09.12.2011 **Kieli** Englanti

☐ **Monografia** ☒ **Yhdistelmäväitöskirja (yhteenveto-osa + erillisartikkelit)**

Tiivistelmä

Tämä väitöskirja käsittelee ultrakylmien fermikaasujen fysiikkaa. Kirjassa esitetään teoreettisia ja numeerisia ennustuksia siitä, mitä kaasussa tulee tapahtumaan, kun siihen kohdistetaan radiotaajussäteilyä, muodostetaan suprajohtava Josephsonin liitos, jossa ylös- ja alas-spinien välillä on potentiaali - ero, tai kun sen annetaan vapautua lasereilla ja magneettikentillä muodostetusta loukusta. Käyttämäni numeerinen menetelmä fermikaasujen mallintamiseen on nimeltään time-evolving block decimation algorithm (hajotelma kvanttimekaanisen aikakehityksen laskemiseen).

Laskemalla radiotaajuusspektrejä olemme tutkineet fermionisen supranesteen luonnetta ja viritystiloja. Josephsonin liitoksessa havaitsemamme epäsymmetriset värähtelyt ylös- ja alas-spinejen välillä kyseenalaistavat perinteisen tulkinnan Josepshonin ilmiöstä Cooperin parien koherenttina tunneloitumisena. Tarkastelemalla sähköä eristävän kaasun laajenemista olemme näyttäneet laajenemisfysiikan selittyvän hyvin yksinkertaisella kaksitilamallilla. Ehdotamme uutta ja yksinkertaista koejärjestelyä pitkään etsityn eksoottisen Fulde-Ferrell-Larkin-Ovchinnikov supranesteen havaitsemiseen.

Avainsanat Fermikaasut, suprajuoksevuus, Fermi-Hubbard, TEBD, Kadanoff-Baym, suprajohtavuus, alhaisten lämpötilojen fysiikka, Josephsonin ilmiö, unitaaridynamiikka, FFLO, törmäysdynamiikka.

ISBN (painettu) 978-952-60-4371-5 **ISBN (pdf)** 978-952-60-4372-2

ISSN-L 1799-4934 **ISSN (painettu)** 1799-4934 **ISSN (pdf)** 1799-4942

Julkaisupaikka Espoo **Painopaikka** Helsinki **Vuosi** 2011

Sivumäärä 119 **Luettavissa verkossa osoitteessa** http://lib.tkk.fi/Diss/

Preface

This thesis is a summary of the research I have carried out during the years 2007-2011 in University of Jyväskylä, Helsinki University of Technology, and Aalto University School of Science. The last four years have been a stunning experience driven by constant changes, understanding of how to work in an academic environment, and unparalleled personal growth. The results presented here would not have come together without the team effort and passion of my colleagues, who I will now take the opportunity to thank.

My supervisor and the leader of our group, Prof. Päivi Törmä, deserves more credit that I can express in few words. Her ambition, deep physical intuition, and enthusiasm are second to none in Finland. I feel indebted to her and to Dr. Francesco Massel who has been my closest postgraduate advisor, mentor, and collaborator. Looking back to my Ph.D. studies I recall the encouraging attitude, constructive feedback, and the result-oriented yet positive atmosphere formed by us three working together.

Dr. Jami Kinnunen has contributed hugely to my understanding of many-body physics, and discussions with him and the time he always has had for me have been absolutely priceless. I appreciate Dr. Mikko Leskinen for laying the foundations for the research with the time-evolving block decimation algorithm in our group. Dr. Dong-Hee Kim has been a pleasure to work with and his assistance in particular with computational problems has been a lifesaver on several occasions. Moreover, I want to acknowledge educating and very useful discussions with Dr. Timo Koponen and Mr. Miikka Heikkinen.

Several important people have provided me insight and their counsel during the road to Ph.D., for which I like to thank them. Sincere thank you to Dr. Vesa Apaja, Dr. Reza Bakhtiari, Ass. Prof. Andrew Daley, Mr. Antti-Pekka Eskelinen, Miss Anna Korolyuk, Mr. Tuomas Lahtinen,

Dr. Agnė Mašalaitė, Mr. Olli Nummi, Mr. Tomoki Ozawa, Dr. Sorin Paraoanu, Dr. Ulrich Schneider, Mr. Daniel Zablocki, and Mrs. Laura Äkäslompolo.

I specially recognise Dr. Antti Savinainen for directing and helping me towards the challenges that I have immensely enjoyed.

I have been fortunate to have candid friends outside the academic environment. Their comradeship, help, and the unforgettable experiences shared together have carried me on also during the times of need. Individually, Mr. Glyn Eggar, Mr. Aapeli Kivimäki, Mrs. Valentina Kurikka, Miss Olga Kurikka, Mr. Arkadi Kurikka, Mr. Topi-Pekka Kääriä, Mr. Samuli Lång, Mr. Tomi J. Nyström, Mr. Eero Palomäki, Mr. Douglas O'Rourke, Mr. Gabriel Straub, Mr. Mikko and Mrs. Maiju Tervajoki, and everybody in Team Laardi have my gratitude and earnest respect.

Funding from Teknillisen korkeakoulun säätiö, Emil Aaltosen säätiö, and Finnish Doctoral Programme in Computational Sciences is acknowledged.

Finally, I dedicate this publication to my dearest ones: Mrs. Riitta Kajala, Mr. Jyrki Kajala, Dr. Kaisa Kajala, Mrs. Ireene Kuosmanen, and Miss Tatjana Kurikka.

Espoo, October 31, 2011,

Jussi Kajala

Contents

List of Publications

This thesis consists of an overview and of the following publications which are referred to in the text by their Roman numerals.

I M.J. Leskinen, V. Apaja, J. Kajala, and P. Törmä, Quasiparticles, coherence and nonlinearity: exact simulations of RF-spectroscopy of strongly interacting one-dimensional Fermi gases, *Physical Review A* **78**, 023602, August 2008.

II M.O.J. Heikkinen, F. Massel, J. Kajala, M.J. Leskinen, G.-S. Paraoanu, and P. Törmä, Spin-asymmetric Josephson effect, *Physical Review Letters* **105**, 225301, November 2010.

III J. Kajala, F. Massel, and P. Törmä, Expansion dynamics in the one-dimensional Fermi-Hubbard model, *Physical Review Letters* **106**, 206401, May 2011.

IV J. Kajala, F. Massel, and P. Törmä, Collision of one dimensional (1D) spin polarized Fermi gases in an optical lattice, *European Physical Journal D,* Advance online publication DOI: 10.1140/epjd/e2011-20081-8, 8 pages, June 2011.

V J. Kajala, F. Massel, and P. Törmä, Expansion dynamics of the Fulde-Ferrell-Larkin-Ovchinnikov state, *Physical Review A* **84**, 041601(R), October 2011.

Other publications to which the author has contributed:

A M.J. Leskinen, J. Kajala, and J.J. Kinnunen, Resonant scattering effect in spectroscopies of interacting atomic gases, *New Journal of Physics* **12**, 083041, August 2010.

Author's Contribution

Publication I: "Quasiparticles, coherence and nonlinearity: exact simulations of RF-spectroscopy of strongly interacting one-dimensional Fermi gases"

The author contributed to the analysis by using the Kadanoff-Baym formalism. The author did the supporting exact diagonalisation simulations and contributed to the writing of the paper.

Publication II: "Spin-asymmetric Josephson effect"

The author, together with M.O.J. Heikkinen, used the Kadanoff-Baym formalism to derive the results presented in the publication. The author contributed to the theoretical discussions, and to the writing of the paper.

Publication III: "Expansion dynamics in the one-dimensional Fermi-Hubbard model"

The author did the numerical simulations for the work, collaborated with the LMU Munich experimental group, and significantly contributed to the theoretical discussions and to the writing of the paper.

Publication IV: "Collision of one dimensional (1D) spin polarized Fermi gases in an optical lattice"

The author did the numerical simulations for the work, significantly contributed to the theoretical discussions, and wrote the paper with the help

of the coauthors.

Publication V: "Expansion dynamics of the Fulde-Ferrell-Larkin-Ovchinnikov state"

The author did the numerical simulations for the work, and significantly contributed to the theoretical discussions and to the writing of the paper.

1. Ultracold Atomic Gases: a Playground for Condensed Matter

1.1 A short background

The field of condensed matter physics studies states of matter in which quantum mechanics and interparticle interactions play an important role, such as the familiar solids, and the more foreign superconductors, ferromagnets, and antiferromagnets. Understanding these states lays the foundation of some applications we use in everyday life: for example fridge magnets, computer hard drives, and the transmission of electric energy. The name of the research field was coined in 1967 by Philip W. Anderson and Volker Heine when they renamed their research group in University of Cambridge from 'Solid-state Theory' to 'Theory of Condensed Matter' [1]. The renaming occurred because it had become apparent that the theories used to describe solids (whose description requires quantum mechanics) were applicable also to quantum fluids. Indeed, the theories that describe e.g. superconductivity in metals (solid) can be used to model superfluidity in e.g. liquid helium and atomic gases (fluid), and vice versa.

In this thesis we will focus on the atomic gases which, regarding fundamental research of physics, have several advantages over solids. They are much easier to control experimentally than metals or other solid state systems. Direct measurements of atomic gases are easy to perform. The density profile, momentum distribution, and excitation spectra are readily accessible. Atomic gases can be made very pure (no defects) and dilute. The gas can be confined in an optical lattice formed by lasers, thus effectively simulating the ionic lattice in metals. However, unlike in metals, the parameters of the lattice can be easily changed. One can adjust the height and geometrical shape of the lattice simply by tuning the laser set-up. Moreover, with a magnetic field one can arbitrarily change the strength of the hyperfine spin interaction between two atoms using a phe-

nomenon called the Feshbach resonance. Finally, and perhaps most importantly, the gas can be cooled to ultracold temperatures (to ca. 100 nK) so that it exhibits quantum mechanical phase coherence which makes the gas superfluid.

Because of the controllability and accurate measurements, cold atomic gases provide a simplified, idealised playground for studying quantum condensed matter physics. We can experiment with them, test and evaluate emerging and established theories, search for new phenomena, and try to explore the physics behind solid-state phenomena that are not well understood, e.g. high temperature superconductivity.

Speaking of the motivation for the research, the pursuit for the room temperature superconductor is one of the holy grails of modern physics (comparable to fusion power, quantum computer or cure for the cancer). A room temperature superconductor would enable transmission of electric energy without dissipation due to resistance, saving large amounts of energy and being a giant leap towards the use of more sustainable sources (e.g. solar power from deserts). Understanding the physics behind superfluids is one of the main goals for the research presented in this thesis. Another motivation is that low-dimensional solids, especially graphene and different nanotubes, have become more attractive for industrial use in solar cells or transistors. By studying ultracold atomic gases we can learn what causes the properties observed in these more complicated systems.

1.2 Experimental highlights

Before discussing the theory required for understanding the results presented in this thesis, let us overview the most important experimental findings of the research field of ultracold atomic gases. The capital experimental highlight of our field has been the realization of the Bose-Einstein condensate in an ultracold Bose gas [2, 3]. The Bose-Einstein condensate, as predicted by Satyendra Nath Bose and Albert Einstein in 1924–25 [4, 5] is a state of matter in which large fraction of particles are in the lowest energy level of the system. To appreciate this, let us briefly discuss the nature of the particles which constitute our universe. The particles can be divided to different classes by many criteria, but the criterion that interests us here is the statistics they follow. All particles

follow either Fermi-Dirac or Bose-Einstein statistics, and are thus named fermions and bosons, respectively. For an equilibrium state with energy E the unnormalised probability for its occupancy is:

$$\frac{1}{e^{\frac{-E}{k_B T}} \pm 1}, \tag{1.1}$$

where the + sign is for fermions and - sign for bosons, k_B is the Boltzmann constant, and T is the temperature. An example distribution is shown in Figure 1.1. Fermions have half-integer spin and bosons have integer spin. Bosons can be elementary, like photons, or composite. Composite bosons are actually built of fermions and their bosonic nature becomes apparent when the energy scale of the phenomenon under observation is much lower than the energy involved in the internal fermionic binding.

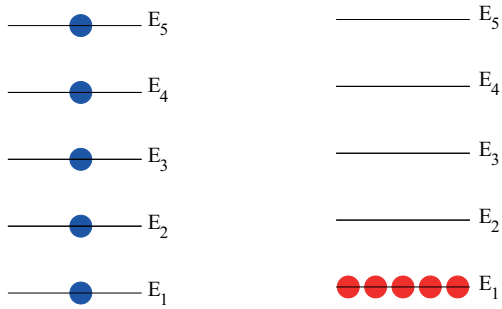

Figure 1.1. Left: The distribution of five identical fermions over five energy levels at zero temperature. Right: The corresponding distribution for five identical bosons. $E_{i+1} > E_i$.

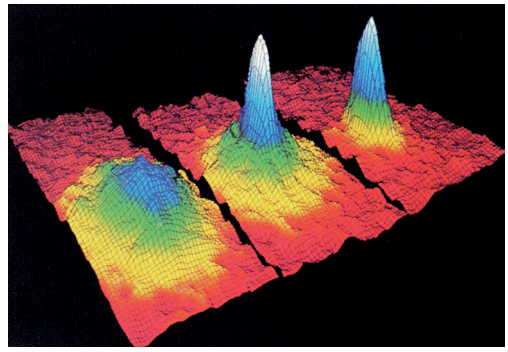

Figure 1.2. Successive occurrence of Bose-Einstein condensation in rubidium. From left to right is shown the atomic distribution in the cloud just prior to condensation, at the start of condensation and after full condensation. Reprinted from The Nobel Foundation 9th September 2001 press release [6].

From Figure 1.1 one sees what happens in Bose-Einstein condensation: a large fraction of particles populate the lowest energy level. This makes it possible for particles in this level to become quantum mechanically coherent, and exhibit phenomena that arise from the coherence, e.g. superfluidity. After 70 years from the prediction of Bose and Einstein, Bose-Einstein condensation was detected in an ultracold Bose gas [2, 3] (see Figure 1.2). Eric Cornell, Carl Wieman, and Wolfgang Ketterle received the 2001 Nobel prize in physics for the observation.

In contrast to bosons, fermions cannot Bose-Einstein condense due to the Pauli exclusion principle. However, two fermions of opposite spins can pair and the pairs, which are composite bosons, can form the condensate. In fact if the fermionic pairing occurs between particles of opposite momentum (k and $-k$) then we speak of Cooper pairs, and we have arrived at the building blocks of one of the most famous condensed matter theories: the Bardeen-Cooper-Schrieffer theory of superconductivity (a.k.a. BCS) [7], which successfully describes the microscopic origin of type-I superconductors. We will return to the BCS theory later, but let us now note that Fermi gas condensates are especially interesting because of their intrinsic connection to solid state superconductors. After the experimental realization of BEC in ultracold gases the next logical step was indeed to see condensation in fermionic systems. In 2003 the groups of Rudolf Grimm [8], Deborah Jin [9] and Wolfgang Ketterle [10] succeeded in producing gases in which fermions formed molecular bosons, and the bosons Bose-Einstein condensed. Later in the same year, the group of Deborah Jin [11] created a true Fermi condensate, i.e. a fermionic condensate without molecular bosons[1]. Since then the study of ultracold Fermi gases has been blooming [12, 13, 14]. So, we are in a relatively young field of physics.

After the Fermi condensate was realised, the focus of the research field was on verifying that the condensate is superfluid. All the experimental observations suggested this, e.g. the pairing gap in the radio frequency spectrum as observed by the group of Rudolf Grimm [15] and theoretically described by the group of Päivi Törmä [16]. The indisputable proof was obtained when vortices were observed in an ultracold Fermi gas in MIT [17]. Truly, superfluids are expected to form quantised vortices under rotation to conserve angular momentum and the lattice of such vortices is what the MIT group saw in a rather spectacular fashion in their 'smoking gun' experiment, see Figure 1.3.

[1]Meaning that there is pairing in the momentum space, c.f. the BCS theory.

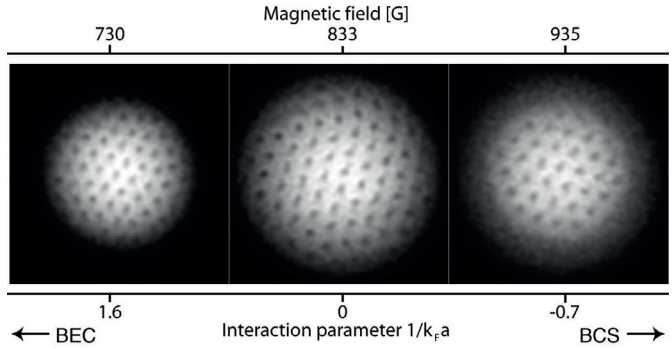

Figure 1.3. The rotating superfluid gas of fermions is pierced with the vortices, which are like mini-tornadoes. Reprinted with permission from M.W. Zwierlein et al., *Vortices and superfluidity in a strongly interacting Fermi gas*, Nature **435**, 1047-1051 (2005).

After these ground-breaking experiments we come swiftly to the current state of affairs. The most notable progress in the last years has been the realization of two-dimensional lattices with the possibility of spatially resolving the population of each lattice site. Pioneered by the groups of Markus Greiner [18], Cheng Chin [19], and Immanuel Bloch and Stefan Kuhr [20], the single-site imaging method has been used for instance to detect short antiferromagnetic spin chains in an ultracold Bose gas [21]. The antiferromagnetic state is worthy of study because in high temperature solid-state superconductors the parent state is antiferromagnetic and it is thought that understanding better the antiferromagnet-superfluid transition provides us valuable information. Indeed, one of the current major goals in the research of ultracold gases is to experimentally realise the antiferromagnetic and ferromagnetic states, especially in a Fermi gas in order to make the system more analogous to solid state equivalents.

Other hot topics in our field at the time of writing are the experimental realization of exotic superfluids, in particular the Fulde-Ferrell-Larkin-Ovchinnikov state (which we will discuss later), universal properties of strongly interacting systems, long-range interactions in dipolar molecules, and dynamics in superfluid systems.

1.3 Modelling systems with a lattice

We are now ready to look more deeply at the physics governing cold atomic gases. In this chapter we will go through well-established models and

theories, finishing off with a more thorough discussion of one-dimensional imbalanced superfluids which do not have a fully established theoretical picture. In the next chapter more advanced methods used to obtain the results of Publications I-V are presented. So, let us begin by considering how physics in a lattice can be modelled.

Just like ions form a lattice for electrons in a solid, an optical lattice for atoms in a Fermi gas can be formed by using lasers. When the temperature T and interactions U compared to the band width J are sufficiently low ($k_BT \ll$ band gap and $\frac{U^2}{J} \ll$ band gap), and long-range interactions between particles can be neglected, a good model for describing the system is the single band Fermi-Hubbard Hamiltonian.

1.3.1 Fermi-Hubbard Hamiltonian

The Fermi-Hubbard Hamiltonian with spin-dependent harmonic trapping potentials included is

$$\begin{aligned} H_{FH} = \; & -U\textstyle\sum_i \hat{n}_{i\uparrow}\hat{n}_{i\downarrow} + V_\uparrow \sum_i (C_\uparrow - i)^2 \hat{n}_{i\uparrow} \\ & + V_\downarrow \textstyle\sum_i (C_\downarrow - i)^2 \hat{n}_{i\downarrow} - J \sum_{i\ \sigma=\uparrow,\downarrow} c^\dagger_{i\sigma} c_{i+1\sigma} + H.c., \end{aligned} \tag{1.2}$$

where U is the on-site interaction strength between opposite spins[2], $V_{\uparrow/\downarrow}$ is the harmonic trap strength for the spin up/down particle, $C_{\uparrow/\downarrow}$ is the centre of the harmonic trap for spin up/down particle, J is the hopping matrix element, $\hat{c}^\dagger_{i\uparrow}$ is a fermionic operator which creates a spin up particle at lattice site i, $\hat{c}_{i\downarrow}$ operator annihilates a down particle at lattice site i, $\hat{n}_{i\uparrow} = \hat{c}^\dagger_{i\uparrow}\hat{c}_{i\uparrow}$ is the density of up particles, and $H.c.$ denotes the Hermitian conjugate of the last term.

The Fermi-Hubbard model is based on the tight-binding model used in describing electron hopping in an ionic lattice, but it is extended to include the on-site interaction U. The underlying assumption is that the localised orbitals that electrons (or atoms in the case of ultracold gases) occupy in each lattice site do not change as a result of the interaction, but instead the population of these orbitals changes due to the competition between the hopping term J and the interaction term U.

We have included the harmonic trap to the model, because it is of particular interest in ultracold atomic gases. Experimentally the harmonic potential is the easiest to realise, provides the means for trapping the gas into a constrained area, and enables also the evaporative cooling scheme

[2]The sign of the interaction has been chosen so that $U < 0$ represents attractive interaction.

[22, 23].

1.3.2 Obtaining the ground state and the time evolution of the system

Let us now look at how the time evolution and the ground state of the system described by the Fermi-Hubbard Hamiltonian is determined. Quantum mechanics is dealt with in the second quantised form, and observables like the time-dependent spin up particle density $n_{i\uparrow}(t)$ are obtained by averaging over the state Ψ of our system: $n_{i\uparrow}(t) = \langle\Psi(t)|\hat{n}_{i\uparrow}|\Psi(t)\rangle$ where the wave-function at time t is obtained in the Schrödinger picture from

$$|\Psi(t)\rangle = e^{-\imath H_{FH} t}|\Psi(t=0)\rangle, \tag{1.3}$$

which is just the Schrödinger equation in a different form, and where $\imath$ is the imaginary unit, H_{FH} is the Fermi-Hubbard Hamiltonian, we have set $\hbar = 1$, and $\Psi(t=0)$ is the initial wave-function.

The initial ground state $\Psi(t=0)$ of the system can be obtained by starting from a guess state Φ, if the guess state is not orthogonal to the ground state, by determining

$$|\Psi(t=0)\rangle = \lim_{\tau\to\infty} \frac{e^{-\tau\hat{H}_{FH}}|\Phi\rangle}{||e^{-\tau\hat{H}_{FH}}|\Phi\rangle||}, \tag{1.4}$$

where τ is analogous to imaginary time when compared to obtaining the time evolution from the Schrödinger equation as discussed above. Indeed, when discrete successive time steps are used to numerically determine the ground state via Equation 1.4 the method is called 'Imaginary time propagation'. Similarly, solving the Schrödinger equation 1.3 numerically this way is called 'Real time propagation'.

Equation 1.4 can be proven by writing Φ in the eigenbasis of the Hamiltonian, i.e. $\Phi = \sum_i c_i|\phi_i\rangle$, where $c_i \in \mathbb{C}$ and $\hat{H}_{FH}|\phi_i\rangle = E_i|\phi_i\rangle$. Then $e^{-\tau\hat{H}_{FH}}|\Phi\rangle = \sum_i e^{-\tau E_i} c_i|\phi\rangle$ and in the limit $\tau \to \infty$ only the ground state is left[3].

Next, we will consider a simple two-site system within the theoretical framework laid above. The two-site system recurs in several different physical systems, and it has been used to analyse the results of the numerical simulations in Publications III-IV.

[3]Unless $c_0 = 0$ which means that the ground state is orthogonal to the guess state.

1.3.3 The two-site system

The two-site Fermi-Hubbard system is analytically solvable (the solution is generally called 'the Hubbard Dimer'), and we go through the solution here in detail. Specifically, the time-evolution of the system with an initially empty state $|\emptyset\rangle$ in the left lattice site and a doublon $|\uparrow\downarrow\rangle$ in the right lattice site without the harmonic trapping potential (for definitions see Equation 1.5) is solved. The time-evolution will tell us about how the initial pair breaks and later we will find out that this pair-breaking mechanism is also applicable to more complicated systems.

As usual, the problem is solved by first expressing the initial state in the eigenbasis of the Hamiltonian, then applying the time evolution using Equation 1.3, and finally determining the overlap between the unpaired state and the time-evolved state. So there is a two-particle basis, and the Fermi-Hubbard Hamiltonian conserves the number of particles. Due to the anticommutation relations, a given order for the application of fermionic operators must be chosen

$$\begin{aligned} |\uparrow,\downarrow\rangle = c^\dagger_{1\uparrow}c^\dagger_{2\downarrow}|0\rangle, \quad |\downarrow,\uparrow\rangle = c^\dagger_{1\downarrow}c^\dagger_{2\uparrow}|0\rangle, \\ |\uparrow\downarrow,\emptyset\rangle = c^\dagger_{1\uparrow}c^\dagger_{1\downarrow}|0\rangle, \quad |\emptyset,\uparrow\downarrow\rangle = c^\dagger_{2\uparrow}c^\dagger_{2\downarrow}|0\rangle, \end{aligned} \tag{1.5}$$

where $|0\rangle = |\emptyset,\emptyset\rangle = |\emptyset\rangle_1|\emptyset\rangle_2$, 1 denotes the left lattice site, and 2 the right lattice site. The Hamiltonian can be divided to the hopping part and the interaction part

$$\begin{aligned} H_{FH} &= H_J + H_{int} \\ H_J &= -J\left(c^\dagger_{1\uparrow}c_{2\uparrow} + c^\dagger_{1\downarrow}c_{2\downarrow}\right) + H.c. \\ H_{int} &= -U\sum_{i=1,2} n_{i\uparrow}n_{i\downarrow}. \end{aligned} \tag{1.6}$$

Then

$$\begin{aligned} H_J|\uparrow,\downarrow\rangle &= H_J\, c^\dagger_{1\uparrow}c^\dagger_{2\downarrow}|0\rangle \\ &= -J\left(c^\dagger_{1\downarrow}c_{2\downarrow}c^\dagger_{1\uparrow}c^\dagger_{2\downarrow}|0\rangle + c^\dagger_{2\uparrow}c_{1\uparrow}c^\dagger_{1\uparrow}c^\dagger_{2\downarrow}|0\rangle\right) \\ &= J\left(-|\uparrow\downarrow,\emptyset> -|\emptyset,\uparrow\downarrow>\right), \end{aligned} \tag{1.7}$$

$$H_J|\downarrow,\uparrow> = H_J\, c^\dagger_{1\downarrow}c^\dagger_{2\uparrow}|0\rangle$$

$$\begin{aligned} &= -J\left(c^\dagger_{1\uparrow}c_{2\uparrow}c^\dagger_{1\downarrow}c^\dagger_{2\uparrow}|0\rangle + c^\dagger_{2\downarrow}c_{1\downarrow}c^\dagger_{1\downarrow}c^\dagger_{2\uparrow}|0\rangle\right) \\ &= J\left(|\emptyset,\uparrow\downarrow> + |\uparrow\downarrow,\emptyset>\right), \end{aligned} \tag{1.8}$$

and obviously,

$$\begin{aligned} H_J|\uparrow\downarrow,0> &= H_J\, c^\dagger_{1\uparrow}c^\dagger_{1\downarrow}|0\rangle \\ &= -J\left(c^\dagger_{2\uparrow}c_{1\uparrow}c^\dagger_{1\uparrow}c^\dagger_{1\downarrow}|0\rangle + c^\dagger_{2\downarrow}c_{1\downarrow}c^\dagger_{1\uparrow}c^\dagger_{1\downarrow}|0\rangle\right) \\ &= J\left(-|\uparrow,\downarrow> + |\downarrow,\uparrow>\right), \end{aligned} \tag{1.9}$$

$$\begin{aligned} H_J|0,\uparrow\downarrow> &= H_J\, c^\dagger_{2\uparrow}c^\dagger_{2\downarrow}|0\rangle \\ &= -J\left(c^\dagger_{1\uparrow}c_{2\uparrow}c^\dagger_{2\uparrow}c^\dagger_{2\downarrow}|0\rangle + c^\dagger_{1\downarrow}c_{2\downarrow}c^\dagger_{2\uparrow}c^\dagger_{2\downarrow}|0\rangle\right) \\ &= J\left(-|\uparrow,\downarrow> + |\downarrow,\uparrow>\right). \end{aligned} \tag{1.10}$$

Hence in the 4-dimensional Hilbert space, with the choice of the basis given by Equation 1.5 (writing out H_{int} is trivial), H_{FH} has the following symmetric representation

$$\mathbf{H_{FH}} = \begin{bmatrix} 0 & 0 & -J & -J \\ 0 & 0 & J & J \\ -J & J & -U & 0 \\ -J & J & 0 & -U \end{bmatrix}. \tag{1.11}$$

The Hamiltonian can be rewritten in a basis where it assumes a block-diagonal form

$$\mathbf{H_{bl}} = \left[\begin{array}{cc|cc} 0 & 0 & 0 & 0 \\ 0 & -U & 0 & 0 \\ \hline 0 & 0 & 0 & -2J \\ 0 & 0 & -2J & -U \end{array}\right]. \tag{1.12}$$

This representation corresponds to the following basis vectors

$$\begin{aligned} |T> &= \frac{1}{\sqrt{2}}\left(|\uparrow,\downarrow\rangle + |\downarrow,\uparrow\rangle\right) \\ |D_-> &= \frac{1}{\sqrt{2}}\left(|\uparrow\downarrow,\emptyset\rangle - |\emptyset,\uparrow\downarrow\rangle\right) \\ |S> &= \frac{1}{\sqrt{2}}\left(|\uparrow,\downarrow\rangle - |\downarrow,\uparrow\rangle\right) \\ |D_+> &= \frac{1}{\sqrt{2}}\left(|\uparrow\downarrow,\emptyset\rangle + |\emptyset,\uparrow\downarrow\rangle\right). \end{aligned} \tag{1.13}$$

The upper block of $\mathbf{H_{bl}}$ is already diagonal, and by diagonalizing the lower block, one obtains the eigenvalues

$$\lambda_{\pm} = -U/2 \left[1 \pm \sqrt{1 + \frac{16J^2}{U^2}} \right]. \tag{1.14}$$

Defining

$$\alpha_{\pm} = +\frac{U}{4J} \left[1 \pm \sqrt{1 + \frac{16J^2}{U^2}} \right] \tag{1.15}$$

the eigenvectors corresponding to the lower block eigenvalues can be written as

$$|v_{\pm}> = \frac{1}{\sqrt{1+\alpha_{\pm}^2}} \left(|S\rangle + \alpha_{\pm} |D_+\rangle \right). \tag{1.16}$$

Hence the diagonalised eigenvectors and the corresponding eigenvalues of the Hubbard dimer are given by

$$\begin{aligned}
&\lambda_- = -U/2 \left[1 - \sqrt{1 + \tfrac{16J^2}{U^2}} \right] (<0) && \Leftrightarrow && |v_-\rangle \\
&\lambda_0 = 0 && \Leftrightarrow && |T\rangle \\
&\lambda_U = -U && \Leftrightarrow && |D_-\rangle \\
&\lambda_+ = -U/2 \left[1 + \sqrt{1 + \tfrac{16J^2}{U^2}} \right] (>U) && \Leftrightarrow && |v_+\rangle.
\end{aligned} \tag{1.17}$$

Having diagonalised the Hamiltonian, let us move on to the time dependent problem. The time evolution of an initial pair is desired, and therefore the state

$$|\phi(t=0)> = |\emptyset, \uparrow\downarrow\rangle = \frac{1}{\sqrt{2}} (|D_+\rangle - |D_-\rangle) \tag{1.18}$$

needs to be expressed in the eigenstates of the Hamiltonian in order to apply the time evolution. Writing $|D_+\rangle$ as a superposition of $|v_+\rangle$ and $|v_-\rangle$ gives

$$|\emptyset, \uparrow\downarrow\rangle = \frac{1}{\sqrt{2}} (\theta_+ |v_+\rangle - \theta_- |v_-\rangle - |D_-\rangle), \tag{1.19}$$

where

$$\theta_{\pm} = \frac{(\sqrt{1+\alpha_{\pm}^2})}{(\alpha_+ - \alpha_-)}. \tag{1.20}$$

Finally, the density of the unpaired state n_{un} in the system after the time evolution can be determined. This is given by $n_{un}(t) = \langle \phi(t) | (1 - \hat{n}_{\uparrow\downarrow}) | \phi(t) \rangle$, where $\hat{n}_{\uparrow\downarrow} = \hat{n}_{1,\uparrow\downarrow} + \hat{n}_{2,\uparrow\downarrow}$. Having set $\hbar = 1$, inserting Equation 1.3 we obtain

$$n_{un}(t) = \langle \emptyset, \uparrow\downarrow | e^{\frac{\imath \hat{H}_{FH}}{\hbar}} (1 - \hat{n}_{\uparrow\downarrow}) e^{-\frac{\imath \hat{H}_{FH}}{\hbar}} | \emptyset, \uparrow\downarrow \rangle. \tag{1.21}$$

Substituting Equation 1.19, calculating this gives

$$n_{un}(t) = \frac{8}{16 + \frac{U^2}{J^2}} [1 - \cos(\sqrt{U^2 + 16J^2}t)], \tag{1.22}$$

which determines the time dependence of doublon $\leftrightarrow$ singlet oscillations in the problem.

Let us now reflect on the result (Equation 1.22) obtained. Firstly, the result would be the same if we turned the problem around, starting from the unpaired initial state $|\uparrow, \downarrow\rangle$ and determining the number of doublons as a function of time $n_{\uparrow\downarrow}(t)$ instead. Secondly, the solution is symmetric between $-U$ and U since the U terms in Equation 1.22 are squared. Thirdly, we have assumed here that the time development is coherent, i.e. the system is not measured during the time evolution. Another interesting case is the stroboscopic observation [24] in which the system is repeatedly measured in the intervals of t^*. The stroboscopic observation is relevant for example when external factors interact with the system effectively measuring it repeatedly. Comparing Equation 1.22 to the stroboscopic measurement, $n_{un}(t)$ in the stroboscopic case would be obtained from the binomial distribution representing the collapse of the wave-function at intervals of t^*, see Figure 1.4.

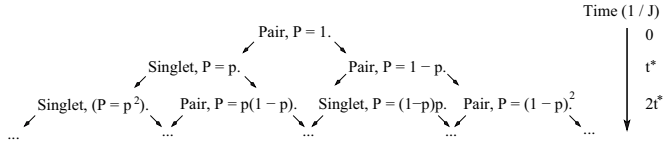

Figure 1.4. The probability triangle for singlets and doublons in a stroboscopic measurement, collapsing the wave-function at repeated intervals t^*. Initially we have a doublon in the right lattice site and hence based on the two-site result $p = \frac{8}{16 + \frac{U^2}{J^2}} [1 - \cos(\sqrt{U^2 + 16J^2}t^*)]$. P denotes the probability.

We have gone through the derivation of the simple two-site system dynamics in detail, and the result obtained here turns out to be important in studying more complicated systems. In fact it is the foundation for the analysis of the results of Publications III - IV, and the result will be referred to below. Before venturing forth, however, we need to look at some of the most known theories of superconductivity, which will be important for understanding the analysis of Publications I, II and V.

1.4 Microscopic theories for superconductivity

We will first go through the widely-used Bardeen-Cooper-Schrieffer (BCS) theory, then look at the extension of the theory to the BCS-BEC crossover (which is of particular interest in ultracold Fermi gases), and finally we will discuss the Fulde-Ferrell-Larkin-Ovchinnikov (FFLO) superfluid that is at the time of the writing under experimental and theoretical focus. The features of the one-dimensional FFLO state are also outlined, as we will examine the 1D FFLO state when discussing the results of Publication V.

Let us make a point here about superconductivity and superfluidity. Superconductivity means flow of electricity without electrical resistance. Superfluidity means flow of liquid without viscosity[4]. Nonetheless, the terms superconductivity and superfluidity are used below sometimes interchangeably, because the theories describing electronic superconductors can be used to describe atom gas superfluids. Moreover, superconducting electrons are also superfluid. But it should be kept in mind that in atomic Fermi gases, however, particles are not charged and thus not superconducting.

1.4.1 BCS

The Bardeen-Cooper-Schrieffer theory is the first microscopic theory of superconductivity. Developed in 1957 [7], it describes superconductivity as an effect caused by the condensation of Cooper pairs. Explaining successfully the properties of type-I ('normal') superconductors such as aluminium and lead, John Bardeen, Leon Neil Cooper and Robert Schrieffer received the Nobel Prize in Physics in 1972 for the theory. We shall now proceed to derive the BCS theory in a uniform infinite lattice.

We start from the Fermi-Hubbard Hamiltonian with a chemical potential term μ which describes the energy cost of adding a particle into the system. It will be needed to fix the average number of particles, noting that the approximations in BCS will change the Hamiltonian so that it does not conserve the particle number. The Hamiltonian is

$$H = -U \sum_i \hat{n}_{i\uparrow}\hat{n}_{i\downarrow} - \mu \sum_i (\hat{n}_{i\uparrow} + \hat{n}_{i\downarrow}) - J \sum_{i\ \sigma=\uparrow,\downarrow} (c^\dagger_{i\ \sigma} c_{i+1\ \sigma} + H.c.). \tag{1.23}$$

[4]There are several more in-depth definitions for superfluidity, none of which is fully comprehensive, and will be not discussed here.

The goal is, again, to diagonalise the Hamiltonian in order to obtain the excitation spectrum (eigenvalues and eigenvectors).

Although the analytic diagonalisation for the simple two-site system above was perhaps trivial, larger systems become difficult to solve analytically. In fact using a computer to obtain an exact solution for large Fermi-Hubbard systems, a system that has the maximum size of only 10-20 lattice sites in one dimension can be solved, with this limit reaching the power of current supercomputers. Furthermore, we are usually interested in superfluids that have at least thousands of particles, so this is not satisfactory. The term that causes the difficulty is the interaction term (indeed, without the interaction term the tight-binding Hamiltonian is easily solvable analytically). Thus, in order to proceed we need to approximate the interaction term in some way. Truly, there are two approximations in BCS, and the first one is that we deal with the interaction term in the mean-field picture only

$$\begin{aligned} H_{int} = -U \quad & \textstyle\sum_i \quad \hat{c}^\dagger_{i\uparrow}\hat{c}_{i\uparrow}\hat{c}^\dagger_{i\downarrow}\hat{c}_{i\downarrow} \\ \approx \quad & \textstyle\sum_i \quad -U\langle\hat{c}^\dagger_{i\downarrow}\hat{c}_{i\downarrow}\rangle\hat{c}^\dagger_{i\uparrow}\hat{c}_{i\uparrow} \\ & \qquad -U\langle\hat{c}^\dagger_{i\uparrow}\hat{c}_{i\uparrow}\rangle\hat{c}^\dagger_{i\downarrow}\hat{c}_{i\downarrow} \\ & \qquad +U\langle\hat{c}^\dagger_{i\downarrow}\hat{c}_{i\downarrow}\rangle\langle\hat{c}^\dagger_{i\uparrow}\hat{c}_{i\uparrow}\rangle \\ & \qquad -U\langle\hat{c}^\dagger_{i\uparrow}\hat{c}_{i\downarrow}\rangle\hat{c}_{i\uparrow}\hat{c}^\dagger_{i\downarrow} \\ & \qquad -U\langle\hat{c}^\dagger_{i\downarrow}\hat{c}_{i\uparrow}\rangle\hat{c}^\dagger_{i\uparrow}\hat{c}_{i\downarrow} \\ & \qquad +U\langle\hat{c}^\dagger_{i\uparrow}\hat{c}_{i\downarrow}\rangle\langle\hat{c}^\dagger_{i\downarrow}\hat{c}_{i\uparrow}\rangle \\ & \qquad +U\langle\hat{c}^\dagger_{i\uparrow}\hat{c}^\dagger_{i\downarrow}\rangle\hat{c}_{i\uparrow}\hat{c}_{i\downarrow} \\ & \qquad +U\langle\hat{c}_{i\uparrow}\hat{c}_{i\downarrow}\rangle\hat{c}^\dagger_{i\uparrow}\hat{c}^\dagger_{i\downarrow} \\ & \qquad -U\langle\hat{c}^\dagger_{i\uparrow}\hat{c}^\dagger_{i\downarrow}\rangle\langle\hat{c}_{i\uparrow}\hat{c}_{i\downarrow}\rangle, \end{aligned} \tag{1.24}$$

where we neglect the first to third terms (these are called the Hartree terms), fourth to sixth terms (called Fock terms), and introduce the BCS mean-field order parameter $\Delta_i = U\langle\hat{c}^\dagger_{i\uparrow}\hat{c}^\dagger_{i\downarrow}\rangle$. Then the total Hamiltonian becomes

$$\begin{aligned} H = \sum_i [& -\mu \sum_{\sigma=\uparrow,\downarrow} (\hat{n}_{i\sigma}) - J \sum_{\sigma=\uparrow,\downarrow} (c^\dagger_{i\ \sigma} c_{i+1\ \sigma} + h.c.) \\ & + \Delta_i \hat{c}_{i\downarrow}\hat{c}_{i\uparrow} + \Delta^*_i \hat{c}^\dagger_{i\uparrow}\hat{c}^\dagger_{i\downarrow}] - \frac{\Delta^2}{U}, \end{aligned} \tag{1.25}$$

which is now analytically diagonalisable and where * denotes the complex conjugate. To gain more physical insight the Hamiltonian is Fourier

transformed to the momentum space and diagonalised there. Fourier transforming the creation and annihilation operators using

$$\begin{aligned} \hat{c}_{i\uparrow} &= \frac{1}{\sqrt{L}} \sum_k e^{\imath i k} c_{k\uparrow}, \\ \hat{c}^\dagger_{i\uparrow} &= \frac{1}{\sqrt{L}} \sum_k e^{-\imath i k} c^\dagger_{k\uparrow}, \end{aligned} \tag{1.26}$$

where $\imath$ is the imaginary unit, and L denotes the total number of lattice sites in the system, one obtains for the chemical potential term in the Hamiltonian

$$\begin{aligned} \mu \sum_{i,\sigma} \hat{n}_{i\sigma} &= \frac{\mu}{L} \sum_{i,k,k'} e^{-\imath i (k-k')} c^\dagger_{k\sigma} c_{k'\sigma} \\ &= \mu \sum_{k\sigma} c^\dagger_{k\sigma} c_{k\sigma}, \end{aligned} \tag{1.27}$$

where the relation $\sum_{i=0}^{i\to\infty} e^{-\imath i(k-k')} = L\delta_{k,k'}$ has been used, δ denoting the Kronecker delta function. For the hopping term one obtains

$$\begin{aligned} J \sum_{i,\sigma} c^\dagger_{i\ \sigma} c_{i+1\ \sigma} &= \frac{J}{L} \sum_{i,k,k'} e^{-\imath [i(k-k')+k]} c^\dagger_{k\sigma} c_{k'\sigma} \\ &= J \sum_k e^{-\imath k} c^\dagger_{k\sigma} c_{k\sigma}, \end{aligned} \tag{1.28}$$

so that combining this term with its Hermitian conjugate gives

$$\sum_{k,\sigma} 2J \cos(k) c^\dagger_{k\sigma} c_{k\sigma}, \tag{1.29}$$

which is nothing but the familiar $2J\cos(k)$ tight-binding term. Finally, for the interaction terms one gets

$$\begin{aligned} \sum_i \Delta_i \hat{c}^\dagger_{i\uparrow} \hat{c}^\dagger_{i\downarrow} &= \frac{1}{L} \sum_{i,k,k'} \Delta_i e^{-\imath i (k+k')} c^\dagger_{k\uparrow} c^\dagger_{k'\downarrow} \\ &= \Delta \sum_k c^\dagger_{k\uparrow} c^\dagger_{-k\downarrow}, \end{aligned} \tag{1.30}$$

where the second fundamental assumption of BCS has been made. Namely, the order parameter Δ is assumed constant. The Hamiltonian in momentum space thus reads

$$H = \sum_{k,\sigma}[2J(1-\cos(k)) - \mu]c^{\dagger}_{k\sigma}c_{k\sigma} + \Delta\sum_{k} c^{\dagger}_{k\uparrow}c^{\dagger}_{-k\downarrow} + \Delta^{*}\sum_{k} c_{k\downarrow}c_{-k\uparrow} - \frac{\Delta^2}{U}, \tag{1.31}$$

where the term $\sum_k 2Jc^{\dagger}_{k\sigma}c_{k\sigma}$ has been added to have the correspondence with the continuous system. To elaborate, in the limit of small momentum the lattice dispersion $2J(1-cos(k))$ now becomes proportional to the free space dispersion $\frac{k^2}{2m}$ (note that $\hbar = 1$). Adding the term is allowed since this just effectively changes the zero of the chemical potential. Now, diagonalising the Hamiltonian gives the eigenvalues and eigenvectors

$$\begin{aligned} E_k \quad &\Leftrightarrow \quad |A\rangle \\ -E_k \quad &\Leftrightarrow \quad |B\rangle, \end{aligned} \tag{1.32}$$

where

$$E_k = \sqrt{(\xi_k - \mu)^2 + \Delta^2}, \tag{1.33}$$

$\xi_k = 2J(1-\cos(k))$ (the non-interacting dispersion relation), $|A\rangle = \alpha^{\dagger}|0\rangle$, $|B\rangle = \beta^{\dagger}|0\rangle$, $|0\rangle$ is the excitation vacuum state, and

$$\begin{aligned} \alpha &= u_k c_{k\uparrow} - v_k c^{\dagger}_{-k\downarrow} \\ \beta &= v_k c^{\dagger}_{k\uparrow} + u_k c_{-k\downarrow}, \end{aligned} \tag{1.34}$$

where $u_k = \frac{1}{\sqrt{2}}\sqrt{1 + \frac{\xi_k - \mu}{E_k}}$ and $v_k = \frac{1}{\sqrt{2}}\sqrt{1 - \frac{\xi_k - \mu}{E_k}}$. The relationships in Equation 1.34 are known as the Bogoliubov transformation. The diagonalised Hamiltonian reads

$$H_{BCS} = \sum_{k} E_k(\alpha^{\dagger}_k\alpha_k + \beta^{\dagger}_k\beta_k - 1) + \xi_k - \frac{\Delta^2}{U}. \tag{1.35}$$

Having obtained the eigenspectrum of the problem, let us give it a little thought. Importantly, the energy of the excitations in the system $E_k = \sqrt{(\xi_k - \mu)^2 + \Delta^2}$ has become gapped. The minimum value that E_k can have is Δ. In fact to create an excitation in the system, a minimum energy equal to 2Δ is required (discussed more below). This is the origin of superconductivity in BCS theory: if one has such an environment that energy required for dissipative excitations is less than twice the energy of the gap (e.g. for thermal dissipation $k_BT \ll 2\Delta$) then these dissipation channels are not excited! Thus, electricity can be conducted without electrical resistance or liquid can flow without friction. One can see that this

is also the reason why superconductivity is seen at low temperatures: it is the region where $k_B T \ll \Delta$.

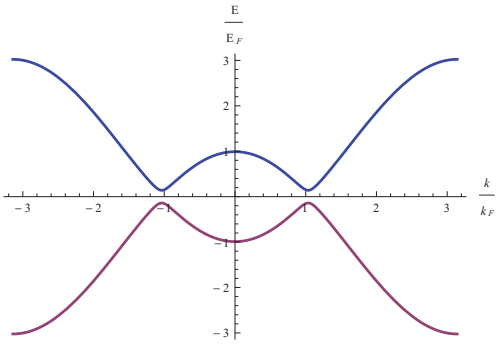

Figure 1.5. The energy cost of breaking a Cooper pair as a function of momentum. We have used $\Delta = 0.14E_F$, $\mu = 0.98E_F$, E_F is the Fermi energy, and both the momentum and energy plotted are in Fermi units as well. Blue graph represents the E_k excitations and the red graph $-E_K$ excitations, as defined in Equation 1.32.

What is the reason for the appearance of the gap? The crucial steps occur in the initial mean-field formulation and in Equation 1.30 when it is assumed that Δ does not depend on the position. The latter effectively pairs an up particle having momentum k with a down particle having momentum $-k$, enforced by the Kronecker delta relation. Thus a Cooper pair composed of particles of opposite momenta is created. The Cooper pairs all have zero momentum and are composite bosons. Actually in the above formalism we do not explicitly see the Cooper pairs, we see only the energy spectrum (Equation 1.33, plotted in Figure 1.5) which tells us how much energy it costs to break a Cooper pair with constituent momenta k and $-k$ from the condensate.

Now, from Equation 1.35 one sees that the ground state of the BCS Hamiltonian is the vacuum state for α and β. Indeed, this state is the BCS condensate which we are after:

$$|BCS\rangle = \prod_k (u_k + v_k c^\dagger_{k,\uparrow} c^\dagger_{-k,\downarrow})|0\rangle, \tag{1.36}$$

where we notice that the intuitive meaning of v_k^2 is the probability of having a Cooper pair at momentum k and the meaning of u_k^2 is the probability of not having it. From the ground state we can determine the energy cost of creating an excitation to the system,

$$\begin{aligned} E_{min} &= \langle BCS|\alpha_k \hat{H}_{BCS}\alpha_k^\dagger|BCS\rangle \\ &\quad -\langle BCS|\hat{H}_{BCS}|BCS\rangle \\ &= 2E_k \\ &= 2\sqrt{(\xi_k-\mu)^2+\Delta^2} \geq 2\Delta. \end{aligned} \tag{1.37}$$

Thus the minimum energy for creating an excitation in the system is 2Δ as discussed above, and we note that it does not matter whether the excitation is of the form $\alpha^\dagger$ or $\beta^\dagger$ as from the form of Equation 1.35 one sees that their effect is the same.

An alert reader might notice that the value of either the gap Δ or the chemical potential μ is not known. What is left to do is to solve these, given the interaction, by what is known as self-consistent solution of the gap and number equations. The number equation for up particles is

$$\begin{aligned} N_\uparrow &= \sum_k \langle c_{k,\uparrow}^\dagger c\dagger_{k,\uparrow}\rangle \\ &= \sum_k \langle (u_k\alpha_k^\dagger + v_k\beta_k)(u_k\alpha_k + v_k\beta_k^\dagger)\rangle \\ &= \sum_k u_k^2\langle \alpha_k^\dagger\alpha_k\rangle + v_k^2\langle\beta_k\beta_k^\dagger\rangle \\ \Rightarrow N_\uparrow &= \sum_k u_k^2 n_F(E_k) + v_k^2 n_F(-E_k), \end{aligned} \tag{1.38}$$

where $n_F(E) = \frac{1}{e^{-\frac{E}{k_BT}}+1}$ and the number equation of down particles is not needed as there are the same number of up and down particles in BCS. The gap equation is

$$\begin{aligned} \Delta &= U\langle c_{i,\uparrow}^\dagger c_{i,\downarrow}^\dagger\rangle \\ &= U\langle \sum_{k,k'} e^{-\imath(k+k')i} c_{k,\uparrow}^\dagger c_{k',\downarrow}^\dagger\rangle \\ &= U\sum_k \langle c_{k,\uparrow}^\dagger c_{-k,\downarrow}^\dagger\rangle \\ &= U\sum_k \langle (u_k\alpha_k^\dagger + v_k\beta_k)(-v_k\alpha_k + u_k\beta_k^\dagger)\rangle \\ &= U\sum_k u_k v_k(\langle\alpha_k^\dagger\alpha_k\rangle + \langle\beta_k\beta_k^\dagger\rangle) \\ &= U\sum_k u_k v_k(2n_F(E_k)-1), \end{aligned} \tag{1.39}$$

and because $u_k v_k = -\frac{\Delta}{2E_k}$ the final form of the gap equation becomes

$$1 = -U \sum_k \frac{(1-2n_F(E_k))}{2E_k}. \tag{1.40}$$

One starts with an initial guess for Δ and μ, inputs these guesses into the number equation, allows these two to change in order to obtain a solution to the number equation, so that new values for Δ and μ are obtained. These values are subsequently substituted into the gap equation, and again new values of Δ and μ are acquired. The procedure is repeated until the values of Δ and μ do not any longer change in the iteration, and then the correct values for the given interaction have been reached. Note that when implementing the self-consistent solution numerically, one needs to express the number of up particles using the Fermi momentum (the relationship depends on the dimensionality), and the number and gap equations need to be written in Fermi units ($E = \frac{E^*}{E_F}, k = \frac{k^*}{k_F}$), the starred quantities denoting the original units.

At finite temperature one finds that above the critical temperature T_c the self-consistent solution gives $\Delta = 0$. Thus, the method allows for the determination of the superfluid-normal transition.

Having covered perhaps the most important aspects of the BCS theory in a lattice (we refer the reader to [25] for more detail), we are ready to look at the BCS-BEC crossover in ultracold Fermi gases.

1.4.2 The mean-field BCS-BEC crossover

In this section we will digress from the lattice models and consider the free space (continuum) case. Understanding continuum physics is very important, as at the moment most of the experiments are done without the lattice, although the trend seems to be moving towards lattice experiments. We will try to point out things that are different in continuum compared to the lattice and hopefully this comparison will be for the benefit of the reader. Thus, let us discuss the continuum BCS-BEC crossover, which is among the most intriguing phenomena occurring in ultracold Fermi gases. The two-component continuum Hamiltonian is

$$\begin{aligned} H = & \int d\mathbf{r} \sum_i \psi_i^\dagger(\mathbf{r})(-\frac{\nabla^2}{2m} - \mu_i)\psi_i(\mathbf{r}) \\ & + \frac{1}{2}\int d\mathbf{r} \int d\mathbf{r}' \sum_{i\neq j} V_{ij}(\mathbf{r}-\mathbf{r}')\psi_i^\dagger(\mathbf{r})\psi_j^\dagger(\mathbf{r}')\psi_j(\mathbf{r}')\psi_i(\mathbf{r}) \end{aligned} \tag{1.41}$$

where $\psi_i(\mathbf{r})$ and $\psi_i^\dagger(\mathbf{r})$ are the fermionic field operators annihilating and creating a state i, respectively, where $i = \uparrow, \downarrow$ (we will explain soon what these spin states actually mean), and $V_{ij}(\mathbf{r} - \mathbf{r}')$ depicts the form of the interaction potential between the different spins. Usually one approximates V with a contact potential $V_{ij}(\mathbf{r} - \mathbf{r}') = U_c\delta(\mathbf{r} - \mathbf{r}')$ and then integrates out the $\mathbf{r}'$ coordinate. U_c is then the interaction strength with the subscript c denoting that the question is about a continuum variable.

One of the most interesting parameters that can be changed in ultracold atomic gases is the interaction strength U_c between the atoms of different spin. This sounds as spectacular as it is: imagine having a means to change the strength of the Coulomb interaction by turning the knob of the measurement apparatus. Resonant phenomena, however, are not scarce. We can indeed find the resonant frequency of, for example, a jelly and by drumming the jelly with this frequency it shatters to pieces (a common experiment done in physics labs). A similar resonance phenomenon occurs in the hyperfine spin states of ultracold atomic gases. Before elaborating on the phenomenon which is called the Feshbach resonance [26, 27], let us briefly discuss the hyperfine spin states.

Above, we have discussed systems with up and down spins, like electrons. What we have instead in atomic gases is the hyperfine spin (F) structure of the atoms which is caused by the interaction between the nuclear spin (I) and the total electron angular momentum (J): $\mathbf{F} = \mathbf{I} + \mathbf{J}$. Nonetheless, in ultracold gas experiments one often has only two hyperfine states occupied. If only two hyperfine states are occupied then we can relabel the states as spin up and down and use all the two-component analysis discussed above. Because of this similarity, we use the terms spin and hyperfine spin interchangeably. Also the term pseudospin is frequently used. What is interesting though is that also systems with more than two hyperfine spin components can be created in cold atomic gases, and in fact the multi-component gases are studied by many groups [28, 29, 30, 31, 32, 33, 34, 35, 36, 37, 38, 39].

Coming back to the Feshbach resonance, this phenomenon occurs because there is a bound state between the two hyperfine spin states. Actually, the ground state of the ultracold gas is a metal (the gas is initially produced by evaporating particles from a metal body), but the gas is just so dilute ($10^{19}\frac{particles}{m^3}$, compared to air at room temperature with $10^{27}\frac{particles}{m^3}$) that three-body recombination processes are rare. The three-body recombination is further suppressed by the Pauli exclusion princi-

ple, and therefore in the time scale of the experiments (seconds) the system stays in the metastable gas state. Two-body recombination, however, can occur in the time scale of the experiments. The particles of opposite spin can form a bound state, a molecule. The Feshbach molecules, being composite bosons, can Bose-Einstein condense. Feshbach resonances that produce many of these molecules are known as narrow, and they have been studied with interest [40]. Nevertheless, commonly the goal is not to have a gas of molecules, but one wants to study the fermionic gas instead. This is possible with broad Feshbach resonance in which the formation of Feshbach molecules is suppressed due to time scale and energy restrictions, and what happens instead is that the presence of the bound state renormalises (changes) the spin-spin interaction strength between two free particles.

Let us elaborate further on the above discussion. What makes the spin interaction controllable is that one can change the energy of the bound state (E_B) with respect to the energy of two free particles (E_F) of different spin by exposing the system to an external magnetic field (**B**). The energy changes at the resonance so that $E_B - E_F \propto B - B_0$, where B_0 is the resonance position. From the first order perturbation theory point of view the amplitude (a) of the two particles scattering to the bound state is $a \propto \frac{1}{E_B - E_F}$. In the case of a broad Feshbach resonance the particles, due to energy and time scale restrictions, cannot stay in the bound state[5] and thus the bound state just acts as a virtual intermediate state which renormalises the free particle scattering length with $a \propto \frac{1}{E_B - E_F} \propto \frac{1}{B - B_0}$. Therefore, by simply tuning the magnetic field all values of the scattering length can be reached, and in particular when $E_B \to E_F$ the scattering length diverges! This is the idea of the Feshbach resonance, and we refer the reader to [12, 13, 14, 42, 43, 44, 45, 46] for more detail.

The point at which the scattering length diverges, the infinite interaction range, is known as 'the unitarity regime'. The unitarity regime in fermionic atom gases is experimentally very interesting [47, 48, 49, 50], and it turns out that the only relevant length scale in this regime is determined by the Fermi momentum k_F. The unitarity regime might not be that radical as it seems. The interaction which becomes infinitely strong is the two-body interaction, but this does not tell us about the many-body

[5]Some fraction of particles do stay in the bound state also in a broad Feshbach resonance. In fact, very recent findings [41] suggest that within the time scale of $10E_F^{-1}$ where E_F is the Fermi energy and $\hbar = 1$ particles occupy the bound state to a large extent.

interactions which give the real response of the system. However, the research of the unitarity regime is made more interesting also by the fact that it is thought to be analogous to other strongly correlated systems, for example the quark-gluon plasma also studied in collisions in the Large Hadron Collider in CERN [51, 52].

Feshbach resonances are not necessarily used in lattice experiments. What matters in the case of the lattice is the ratio between J and U and this can be changed by simply changing the lattice height, reaching all the values of $\frac{U}{J}$ in this way. In contrast, in continuum experiments the interaction U_c is compared to the kinetic term with the pre-factor $\frac{1}{2m}$[6], and the ratio of these is changed via the Feshbach resonance. In a Feshbach resonance, the two-body scattering length a determines the strength of the spin-spin interaction U_c. To solve the full many-body response of the system with the presence of the bound state in order to obtain a relationship between a and U_c is a formidable task. Indeed, the theory which establishes the relationship is called the T-matrix scattering theory and it has not been analytically solved for general values of a and U_c. All the limits of the theory (in particular the limit when the scattering length diverges) are not yet well understood. However, the weakly attractive interaction limit of the theory is well established, the relationship in this limit being

$$U_c = \frac{4\pi a}{m}. \tag{1.42}$$

In obtaining this formula, a contact interaction (delta function potential) between the spins has been assumed, which creates divergences that need to be corrected. For example the BCS gap equation in the continuum case diverges for large k and needs to be modified in order to remove the divergence. In fact the T-matrix theory corrects for the divergence, and this is where the regularization of the BCS gap equation in continuum rigorously comes from.

Although Equation 1.42 holds only in the weakly interacting limit, a widely-used model for the whole crossover (a going from $-\infty$ to ∞) is that one simply uses the continuum BCS gap and number equations with the relationship between the scattering length and the interaction given by Equation 1.42. We note that the continuum BCS gap and number equations are actually the same as the lattice ones[7], with the only changes

[6] $\hbar = 1$.

[7] Thus in the continuum case regularising the gap equation by the T-matrix analysis simply returns the gap equation to the lattice form, which is not surprising.

being replacing the summation by integration and the lattice dispersion $1 - cos(k)$ by continuum dispersion k^2. Indeed, we can attain the values of Δ and μ for all interaction strengths U_C by the self-consistent solution of gap and number equations and doing so we have arrived at what is known as the mean-field BCS-BEC crossover theory, first suggested by [53, 54, 55].

The experiments in Feshbach resonant Fermi gases confirm that there is a smooth crossover from the BEC to the BCS side. We refer the intrigued reader to Chapter 6 of [14] for an in-depth experimental review, and point out that the crossover theory discussed above seems to be a reasonable approximation when the temperature is much less than the critical temperature for the superfluidity. The experiments are often done at the unitarity, because there the interaction strength is the strongest, and therefore the critical temperature for superfluidity is the highest. Indeed, experiments in the BCS limit have not yet reached a temperature low enough for superfluidity. However, the experimental measurements of Δ and μ at the unitarity can be compared to the values predicted by the 3D continuum mean-field BCS-BEC crossover. The results of the mean-field BCS-BEC theory for a different interactions are presented in Figure 1.6 and comparing $\mu(a \to \infty)$ to the experiments and to Quantum Monte Carlo numerics is shown in Figure 1.7.

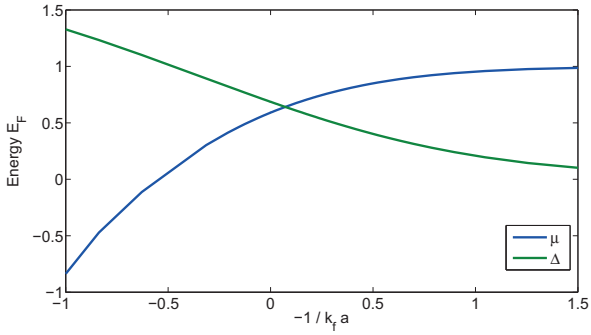

Figure 1.6. The values of Δ (in green) and μ (in blue) obtained from solving the gap and number equations self-consistently for different values of the interaction $U_c = \frac{4\pi a}{m}$.

Finally, let us discuss the mean field BCS-BEC crossover in the light of Figure 1.7. It is somewhat surprising that the value obtained in the mean field BCS-BEC crossover matches the experimental observations

To elaborate, the regularisation is physically the same as providing high energy cutoff which is provided in lattice.

Theory / experiment	β
BCS mean field	−0.41
QMC	−0.58
ENS Li−6	−0.59
Duke Li−6	−0.49
Rice Li−6	−0.54
Innsbruck Li−6	−0.73
Jila K−40	−0.54

Figure 1.7. The value of chemical potential at unitarity $\mu(a \to \infty) = (1+\beta)E_F$, where E_F is the Fermi energy, as calculated by the BCS-BEC mean field crossover in 3D continuum, Quantum Monte Carlo numerics [56, 57, 58], and as measured in different experiments [59, 60, 61, 62, 63]. All the other experimental results are at finite temperature, but the JILA result is an extrapolation to $T = 0$. The mean-field BCS-BEC crossover theory and Quantum Monte Carlo results have assumed $T = 0$. This table is a shortened summary of the review presented in [59]. Note that the newest experiments indicate that the value of β is lower ($\beta \approx -0.4$). However, since these results are still unpublished we quote here only the older data.

quite well. The fact that the BCS theory seems to provide reasonable estimates for $\mu(a \to \infty)$ and $\Delta(a \to \infty)$ tells us that it cannot be too far from the theory of superfluidity at unitarity.

Now let us take a look at Figure 1.6 and consider what the different regimes mean physically. When the spin interactions are attractive ($U_c < 0$, the right side of Figure 1.6) in the BCS-BEC crossover, we have the BCS side with pairing in momentum space between particles of opposite momenta and condensation of Cooper pairs. In the BEC limit the spin interaction is repulsive ($U_c > 0$, the left side of Figure 1.6), we have pairing in real space, i.e. molecules that have a binding energy μ, and the Cooper pairs which have become molecules in this limit again condense. The unitarity is something in between: pairing has both momentum and real space character.

These remarks close our discussion on the BCS superfluidity and the BCS-BEC crossover, and we are ready to move on to even more uncharted waters. Next we will discuss the Fulde-Ferrell-Larkin-Ovchinnikov superfluid, which is important for understanding non-BCS superfluids, and has not yet been directly observed in an experiment.

1.4.3 The FFLO state

Two independent publications in 1964, one by Peter Fulde and Richard A. Ferrell [64] and the other by Anatoly Larkin and Yuri Ovchinnikov [65], predicted the existence of an imbalanced superfluid whose constituents have non-zero center-of-mass momentum q. By imbalance we mean that there are different number of spin up and spin down particles ($N_\uparrow \neq N_\downarrow$). The superfluid state is called the Fulde-Ferrell-Larkin-Ovchinnikov (FFLO) after its founding fathers. We are interested in the FFLO state because understanding exotic (non-BCS) superfluidity can shed light to the mystery of high temperature superconductors, and to the phenomenon of superfludity and superconductivity in general.

Indeed, realising the FFLO state has been a major goal since creating the first Fermi condensates. Even though indirect measurements in solid-state [66, 67, 68, 69, 70, 71, 72, 73, 74, 75, 76, 77, 78] and in a one-dimensional Fermi gas [79] are in accordance with the existence of the state, the smoking gun signature revealing the FFLO momentum q is lacking. To draw a parallel, it took 70 years to realise the Bose-Einstein condensate since its theoretical prediction, and now we are closing to 50 years during which the Fulde-Ferrell-Larkin-Ovchinnikov (FFLO) state has evaded direct experimental observation. In Publication V we suggest a simple scheme for detecting the FFLO state in one dimension, and let us therefore now discuss the properties of the FFLO.

In contrast to the BCS theory, the order parameter in the FFLO state is not constant. It is instead assumed to have oscillating position-dependence so that $\Delta_i = \Delta e^{iiq}$, where Δ denotes again the amplitude of the order parameter and q is the FFLO momentum, the period at which the order parameter oscillates in space. Therefore, when in Equation 1.30 we Fourier transform the annihilation and creation operators, one can see that the FFLO definition of the order parameter leads to the condition $\delta_{k',-k+q}$ instead of $\delta_{k',-k}$. Physically this means that in BCS theory the Cooper pair is formed of particles with momenta k and $-k$ with the center-of-mass momentum being zero, whereas in the FFLO state the condensate constituents have momenta $k+q$ and $-k$ (or equivalently $k+\frac{q}{2}$ and $-k+\frac{q}{2}$ in the center-of-mass frame). Therefore, the Cooper pairs in the FFLO state have center-of-mass momentum q.

The analysis of the BCS section above can be generalised to take into account FFLO pairing easily. In addition to the change in Δ, spin-dependent

chemical potentials must be introduced ($\mu_\uparrow$ and $\mu_\downarrow$) because the number of up and down particles is different. With these two changes one can repeat the BCS analysis, arriving at the mean-field FFLO theory. Simply, the FFLO state is an extension for BCS to take into account $N_\uparrow \neq N_\downarrow$ and pairing with finite center-of-mass momentum.

Now, a reasonable question to ask is that what kind of pairing then actually takes place, is it BCS, FFLO or something else? Mean-field calculations for a three dimensional sysytem in a lattice suggest that there are several possibilities that can happen in an imbalanced superfluid [80]. The pairing can actually be of BCS type and the excess majority particles which do not fit into the BCS state remain in the normal state. This is called the phase separation (PS). Alternatively, any kind of superfluid pairing can be less favourable than being in the normal state, and then the gas does not form a superfluid. This is a well-known phenomenon which has been experimentally observed also in imbalanced Fermi gases [81], it occurs when the polarisation $P = \frac{N_\uparrow - N_\downarrow}{N_\uparrow + N_\downarrow}$ is increased. The critical polarisation when superfluidity is lost is known as the Chandrasekhar-Clogston limit [82, 83] (used also in the context of critical magnetic fields for breaking superfluidity). Third scenario is that in real space the gas is a homogeneous superfluid, but in momentum space there is phase separation. The scenario is known as the Breached Pair state (BP) and is characterised by gapless excitations. In the case of fixed chemical potentials, the Breached Pair state is a maximum of energy and therefore unstable. Finally, the gas can form the FFLO state with pairs having momentum q.

Nonetheless, in experiments it can be difficult to identify the type of superfluidity. The macroscopic behaviour of the superfluid (flow without friction, formation of vortex lattices) is similar for both FFLO and BCS type of superfluids. Probing the microscopic origin of pair formation in a superfluid is not easy, and commonly one resorts to indirect, and inconclusive, signatures to determine the microscopic state of the superfluid. What we would like to have instead is a clear-cut signal showing the FFLO momentum q.

A quantitative feature that theoretically identifies the nature of the superfluid is the pair momentum correlator n_k, which is given by

$$n_k = \frac{1}{2L} \sum_{i,j}^{L} e^{\imath(i-j)k} C_{ij}, \tag{1.43}$$

where

$$C_{ij} = \langle \Phi | c^\dagger_{i\uparrow} c^\dagger_{i\downarrow} c_{j\downarrow} c_{j\uparrow} | \Phi \rangle, \tag{1.44}$$

and L is the number of lattice sites in the system. The correlator n_k for a BCS state and for a FFLO state are shown in Figure 1.8. The experimental problem for measuring n_k is that one needs to probe the response of the system in order to detect n_k (i.e. for example measuring ground state density profile is not enough), and although there are plenty of suggestions for such probes [84, 85, 86, 87, 88, 89, 90, 91, 92, 93, 94] they have not yet been realised. However, we show that in exotic systems q can be measured in a rather direct way. The above discussion brings us to such an interesting system: the strongly interacting FFLO state in one dimension.

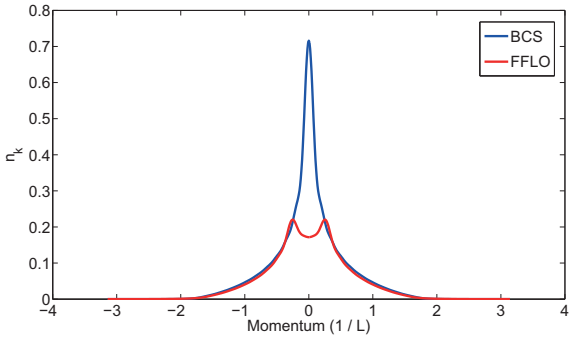

Figure 1.8. The pair momentum correlator n_k plotted for BCS and FFLO states.

1.4.4 The FFLO state in 1D

One-dimensional systems are special by nature. In 1D particles cannot pass each other without interacting, and instead of a Fermi surface there are Fermi points. Fluctuations become non-negligible, mean field theories fail, and excitations of systems are collective instead of single particle like [95]. As an example of a 1D system, imagine two balls that are constrained to move on a line. The balls cannot pass each other or swap places. The position and speed of the other ball necessarily affects the positions on the line that the another ball can reach, since navigating around the other is not possible. So, physics in 1D is quite different to 3D, and one would expect also the nature of superfluidity change. As the BCS and FFLO descriptions are mean-field theories, they are not as such

applicable in one dimension[8].

The crossover from 3D superfluid to 1D superfluid is a field of ongoing research both in theory and experiments [12, 13, 14]. Speaking of the experiments, the 1D setting can be realised in ultracold gases by imposing a two-dimensional optical lattice on the gas in the harmonic trap [79]. Then, if the lattice height is large enough only the lowest energy state in each 2D lattice site is populated, and the gas is therefore confined to move in only one dimension. In this way one produces an array of 1D-tubes. If the coupling between the tubes is vanishing, one has a collection of truly one-dimensional systems, whereas if the coupling is weak but non-zero one says that the system is quasi-1D. Such systems have also been suggested to be promising for the detection of the FFLO state [97, 98]. However, we will focus here on the fully 1D setting, not the quasi-1D one.

Now, a state analogous to the FFLO state exists in 1D. It is analogous in the fundamental microscopic sense that the pairing correlations n_k of this state exhibit a peak at q and therefore the state, although not equivalent to the 3D mean-field FFLO state, is called the 1D FFLO state. As the 1D FFLO state has become the candidate for observing the FFLO pairing with momentum q experimentally, it has recently attracted much theoretical and experimental attention (see [79, 99] and references therein). However, the properties of the state are not yet understood completely. Although in principle systems without the trap in 1D can be analytically solved using a method known as the Bethe Ansatz [100, 101], the Bethe Ansatz solution is often so complicated that it hides the physical meaning behind it. Thus the Bethe Ansatz solution is in many cases used only to verify the results obtained otherwise. The presence of the trap complicates things further. In higher dimensions one can consider the effect of harmonic trapping in the local density approximation (LDA) sense, i.e. dividing the system into intervals and approximating that the trap is constant within these intervals (hence the effective chemical potential in each interval being different). Then, uniform infinite system results are used on each of the intervals. But LDA, being a mean field approach, is a worse approximation in 1D than it is in higher dimensional systems.

Nonetheless, there are several facts that we know for certain, based on Bethe Ansatz, numerical, and conformal field theory considerations (see [79, 99, 102] and references therein). Firstly, the 1D FFLO state is the ground state of the system for all non-zero polarisations at zero

[8] An interesting work [96] compares BCS to the Bethe Ansatz solution in 1D.

temperature. This is in sharp contrast to 3D where the FFLO phase space is quite limited [103, 104, 105]. Also, this means that the Chandrasekhar-Clogston limit in 1D is $P = 1$. Secondly, the FFLO momentum is equal to the difference of the up and down Fermi points: $q = k_{F\uparrow} - k_{F\downarrow}$ so that particles at Fermi surfaces pair with each other analogously to the 3D FFLO. Let us discuss this feature more in detail.

If a 1D box with hard boundaries is considered, the boundary conditions limit the possible excitations of the system into such that the non-interacting n^{th} energy level has momentum $k_n = \frac{n\pi}{L}$, where L is the length of the box. Thus, if we have $N_\uparrow$ up particles we obtain $k_F = \frac{N_\uparrow \pi}{L} \approx n_\uparrow \pi$, where $n_\uparrow$ is the density of up particles. The approximation assumes a constant density in the middle of the box, and is a good approximation unless the particle number is very low. Importantly this means that

$$q = k_{F\uparrow} - k_{F\downarrow} = (n_\uparrow - n_\downarrow)\pi, \tag{1.45}$$

where we have dropped the approximation sign keeping in mind that the equation is not exact for very low (< 10) number of particles. This, obviously, does not provide a means for detecting the FFLO state simply from the density difference as the above relationship does not tell us about pairing (Equation 1.45 holds for the non-interacting case) but rather just that q predicted for the 1D FFLO state is the same as the density difference. Let us then consider how turning on the interactions affect $n_\uparrow - n_\downarrow$ in the trap center. Although turning the spin interactions on can change the occupancy of basis states differently for up and down particles, the linear relationship between k_F and n in 1D makes the effect of the Fermi point rounding on $n_\uparrow - n_\downarrow$ less pronounced than in higher dimensions. Elaborating on this, if the effect of the interactions is to round the population distribution around the Fermi point so that $k_{F\uparrow} \to k_{F\uparrow} + \delta$, $k_{F\downarrow} \to k_{F\downarrow} + \delta$, the effect will cancel when taking the difference $n_\uparrow \pi - n_\downarrow \pi = k_{F\uparrow} + \delta - (k_{F\downarrow} + \delta) = k_{F\uparrow} - k_{F\downarrow}$. Thus, as a first approximation we can assume that Equation 1.45 holds also in the interacting case. This is consistent with experimental and numerical findings ([79, 99] and references therein) showing that $(n_\uparrow - n_\downarrow)\pi$ at the center of the trap also in the interacting case is equal to the FFLO momentum q as predicted.

Based on the above discussion, we are left with the quest for evidence of pairing at q. A setting that might provide the evidence is the strongly interacting limit. In the strongly interacting limit a gas in the 1D FFLO

state becomes a two-fluid gas, the two fluids being paired and unpaired particles [106]. From the two-site system considerations one can see a reason for this in lattice systems: if particles are in a doublon state, the amplitude to singlet conversion is suppressed by $\frac{8}{16+\frac{U^2}{J^2}}$ (see Equation 1.22). If they are in the singlet state, the amplitude to doublon conversion is suppressed by the same factor. Hence the pairing physics in the $U >> J$ limit leads into a two-fluid gas in which the two components (pairs and unpaired particles) do not interact. Bethe Ansatz considerations in continuum [106] show that the two gases form separate Fermi seas.

Now the time has come to turn our attention to the more sophisticated numerical and analytical methods used in obtaining the results in this thesis.

2. Methods

In this section we will discuss the numerical method that has been used to simulate the dynamics of the Fermi-Hubbard Hamiltonian (Equation 1.2) in Publications I - V, and the many-body theory used for calculating the response of the system in Publications I-II. We will start off with the numerical method which is called the time-evolving block decimation algorithm.

2.1 Time-evolving block decimation algorithm

The time-evolving block decimation algorithm, abbreviated TEBD, was developed in 2003 by Guifré Vidal in California Institute of Technology [107]. TEBD is an algorithm used to simulate low dimensional quantum many-body systems with a discrete lattice and low amount of entanglement. In one dimensional systems the amount of the entanglement between the different lattice sites is usually the lowest [108]. Therefore, TEBD is an ideal method for studying one-dimensional spin chains and, more in general, quantum lattice systems. TEBD is closely related to the density matrix renormalisation group (DMRG) method [109] although the implementations of TEBD and DMRG differ [110].

TEBD works for both fermions and bosons, and there are no sign problems involved (c.f. Quantum Monte Carlo methods for fermions). The method is exact when a numerical parameter called the Schmidt number χ is S^L, where S is the number of possible local spin states and L is the size of the lattice. However, in systems with low entanglement the essential physics of the system is retained also with a cutoff for χ and therefore TEBD is known as an essentially exact method. We will come back to this, but let us first focus on explaining how TEBD works. We

have used TEBD to calculate the ground states, time evolution and correlation functions of systems described by the Fermi-Hubbard Hamiltonian. The simulation steps needed to obtain these correspond to the imaginary time propagation, the real time propagation, and pair correlation C_{ij}, respectively (i.e. Equations 1.3, 1.4, and 2.14). Having discussed each in the previous chapter, we will next overview how the algorithm is used for determining them.

2.1.1 The idea of the TEBD algorithm

The basic idea of TEBD is to reduce the Hilbert space in a controlled manner. When in the previous chapter we went through the analytical solution of the two-site system and the BCS theory it was mentioned that two-component Fermi-Hubbard systems with more than 10-20 lattice systems cannot be today solved exactly even with the best supercomputers. Thus, approximations are needed to scale down the problem. Unlike in e.g. the BCS theory, the approximations in TEBD do not involve estimating the interaction term by e.g. the mean-field assumption. In contrast, in TEBD the Hilbert space is truncated using the Schmidt Decomposition and Singular Value Decomposition (the latter is abbreviated SVD). Importantly, it turns out that the coefficients of the successive terms involved in the series decompositions decay exponentially when there is low entanglement between the different lattice sites of the system. This enables the truncation of the decompositions at χ and keeping the essential physics in the description.

For the purpose of understanding how TEBD works, we will go through how to write the quantum mechanical state, how operations are performed on it, and what is involved in the abovementioned decompositions and their truncation. Let us begin by writing the state. Generally, any state in a lattice can be written in the product form

$$|\Psi\rangle = \sum_{\{s_1\},\{s_2\},...,\{s_L\}} c_{s_1 s_2 ... s_L} |s_1\rangle |s_2\rangle ... |s_L\rangle, \tag{2.1}$$

where the states $\{s_i\}$ make the local Hilbert space basis of size S, and L is the number of lattice sites. For the two component Fermi-Hubbard model the states $\{s_i\}$ are $|\emptyset\rangle$, $|\uparrow\rangle$, $|\downarrow\rangle$, $|\uparrow\downarrow\rangle$ and thus $S = 4$. Now, in order to use the form shown in Equation 2.1 one needs a way for determining the coefficients $c_{s_1 s_2 ... s_L}$, which is why we turn to the Schmidt Decomposition. The Schmidt theorem states that [111] one can divide the full quantum

system $|\Psi\rangle$ into two subsystems

$$|\Psi\rangle = \sum_{i}^{\chi} \lambda_i |\Psi_i\rangle_A \otimes |\Psi_i\rangle_B, \tag{2.2}$$

where χ is the Schmidt number. So let us divide the spin chain between sites 1 and 2 so that on the left side one has the first site and on the right side there is the rest of the chain

$$|\Psi\rangle = \sum_{\alpha_1}^{\chi} \lambda_{\alpha_1}^{[1]} |\Psi_{\alpha_1}^{[1]}\rangle \otimes |\Psi_{\alpha_1}^{[2...L]}\rangle, \tag{2.3}$$

and then the spin chain is divided between sites 2 & 3,

$$|\Psi\rangle = \sum_{\alpha_1\alpha_2}^{\chi} \lambda_{\alpha_1}^{[1]} |\Psi_{\alpha_1}^{[1]}\rangle \otimes \lambda_{\alpha_2}^{[2]} |\Psi_{\alpha_1\alpha_2}^{[2]}\rangle \otimes |\Psi_{\alpha_2}^{[3...L]}\rangle, \tag{2.4}$$

then between sites 3 & 4, and so on. Moreover, the states $|\Psi^{[i]}\rangle$ are mapped to the local spin basis $\{s_i\}$ so that

$$|\Psi_{\alpha_i\alpha_j}^{[i]}\rangle = \sum_{\{s_i\}} \Gamma_{\alpha_i\alpha_j}^{[i]\{s_i\}} |s_i\rangle |\alpha_j\rangle, \tag{2.5}$$

where i is the lattice site index, see Figure 2.1.

Doing the division for the whole chain one obtains the coefficients for the Matrix Product State we were after:

$$|\Psi\rangle = \sum_{\{s_1\},\{s_2\},...,\{s_L\}} c_{s_1 s_2 ... s_L} |s_1\rangle |s_2\rangle ... |s_L\rangle, \tag{2.6}$$

where

$$\begin{aligned} c_{s_1 s_2 ... s_L} \quad = \quad & \Gamma_{\alpha_1}^{[1]\{s_1\}} \lambda_{\alpha_1}^{[1]} \Gamma_{\alpha_1\alpha_2}^{[1]\{s_2\}} \lambda_{\alpha_2}^{[2]} \\ & ... \Gamma_{\alpha_L - 1 \alpha_L}^{[L-1]\{s_{L-1}\}} \lambda_{\alpha_L}^{[L]} \Gamma_{\alpha_L}^{[L]\{s_L\}}, \end{aligned} \tag{2.7}$$

and summations for repeated indices (s_i and α_i for each lattice site) are omitted for clarity. Restating what λ and Γ mean, λs are the coefficients of the Schmidt decomposition and Γs come from mapping the $|\Psi^{[i]}\rangle$ states onto the local spin basis.

Thus the state is now in the form used by TEBD. It is emphasised that in Equation 2.2 the Schmidt number χ appeared, and the idea is to truncate the series expansions at χ, making the problem computationally solvable. Moving on to explaining how operations are done on the state of the above

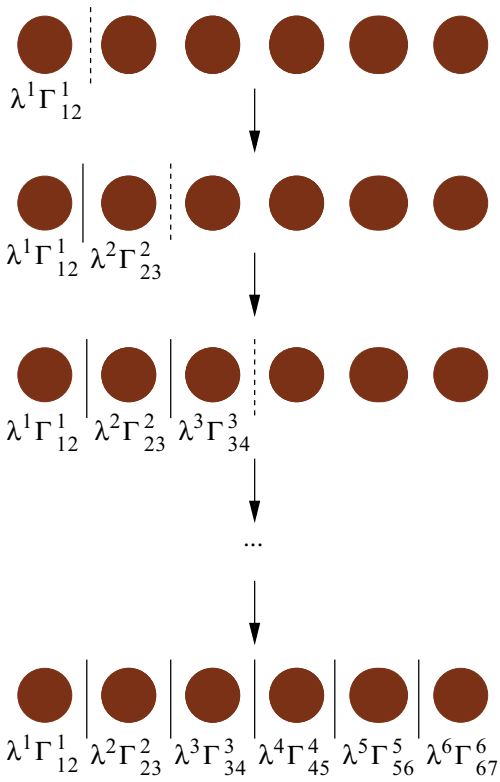

Figure 2.1. Schmidt decomposing the lattice chain one by one.

form, let us first take a look at how on-site operations are done. On-site operations in the local spin basis denoted by $\hat{\mathbf{U}}$ are simple. Their effect is to update the Γ matrices via the formula

$$\Gamma^{[i]\{s_i\}}_{\alpha_{i-1}\alpha_i} \rightarrow \tilde{\Gamma}^{[i]\{s_i\}}_{\alpha_{i-1}\alpha_i} = \sum_{\{s_i'\}} \mathbf{U}^{\{\mathbf{s_i}\}}_{\{\mathbf{s_i'}\}} \Gamma^{[i]\{s_i'\}}_{\alpha_{i-1}\alpha_i}. \tag{2.8}$$

So, only Γs on sites which are operated upon are affected, and the product state has the same size after the operation. An example of an on-site operation is $c^\dagger_{i\uparrow}$ which makes the elements in Γs with $s_i =\uparrow$ and $s_i =\uparrow\downarrow$ zero at lattice site i and turns the elements in Γs with $s_i = \emptyset$ and $s_i =\downarrow$ into the corresponding elements with $s_i =\uparrow$ and $s_i =\uparrow\downarrow$, respectively.

The nearest-neighbour operations denoted by $\hat{\mathbf{V}}$, however, are not that straightforward. Their effect is

$$\hat{\mathbf{V}}|\Psi\rangle \rightarrow \sum_{\alpha_{i-1},\alpha_{i+1}}^{\chi} \sum_{\{s_i\},\{s_{i+1}\}} \theta^{\{s_i\}\{s_{i+1}\}}_{\alpha_{i-1}\alpha_{i+1}} |\Psi^{[1\ldots i-1]}_{\alpha_{i-1}}\rangle |s_i\rangle |s_{i+1}\rangle |\Psi^{[i+2\ldots L]}_{\alpha_{i+1}}\rangle, \tag{2.9}$$

where

$$\theta^{\{s_i\}\{s_{i+1}\}}_{\alpha_{i-1}\alpha_{i+1}} = \sum_{\alpha_i}^{\chi} \sum_{\{s_i^{'}\}\{s_{i+1}^{'}\}} \mathbf{V}^{\{\mathbf{s_i}\}\{\mathbf{s_{i+1}}\}}_{\{\mathbf{s_i^{'}}\}\{\mathbf{s_{i+1}^{'}}\}} \lambda^{[i-1]}_{\alpha_{i-1}} \quad \Gamma^{[i]\{s_i^{'}\}}_{\alpha_{i-1}\alpha_i} \lambda^{[i]}_{\alpha_i} \quad \Gamma^{[i+1]\{s_{i+1}^{'}\}}_{\alpha_i\alpha_{i+1}} \lambda^{[i+1]}_{\alpha_{i+1}}. \tag{2.10}$$

The $\mathbf{V}^{\{\mathbf{s_i}\}\{\mathbf{s_{i+1}}\}}_{\{\mathbf{s_i^{'}}\}\{\mathbf{s_{i+1}^{'}}\}}$ term above cannot be straightforwardly incorporated into new λs and Γs after the $\{s_i^{'}\}\{s_{i+1}^{'}\}$ summation in analogy to the onsite case. The reason for this is that the nearest-neighbour term couples by definition the spin states $\{s_i\}$ and $\{s_{i+1}\}$ between the two neighbouring lattice sites. As a matter of fact, the $\mathbf{V}^{\{\mathbf{s_i}\}\{\mathbf{s_{i+1}}\}}_{\{\mathbf{s_i^{'}}\}\{\mathbf{s_{i+1}^{'}}\}}$ term has increased the size of the local Hilbert space at these sites by the factor of S. To prevent the numerically unstable increase of the Hilbert space, the state needs to be returned to the original $\lambda\Gamma\lambda\Gamma$ - form, which means cutting the increased local Hilbert space by the factor of S. The cutting is achieved by doing a singular value decomposition (SVD) on $\theta^{\{s_i\},\{s_{i+1}\}}_{\alpha_{i-1}\alpha_{i+1}}$.

Using the SVD-theorem the term $\theta^{\{s_i\},\{s_{i+1}\}}_{\alpha_{i-1}\alpha_{i+1}}$ is written in the form $\theta = ADB^{\dagger}$, where A and B, divided by original λs at the sites $i-1$ and $i+1$, respectively, give the new Γ matrices and the diagonal elements of D give the new λ vector. Only terms up to χ in the summation are kept in the SVD and thus one obtains the state in the desired form

$$\hat{\mathbf{V}}_{\mathbf{i,i+1}}|\Psi\rangle \rightarrow \sum_{\alpha_{i-1}\alpha_i\alpha_{i+1}}^{\chi} \lambda^{[i-1]}_{\alpha_{i-1}} \tilde{\Gamma}^{[i]\{s_i\}}_{\alpha_{i-1}\alpha_i} \tilde{\lambda}^{[i]}_{\alpha_i} \tilde{\Gamma}^{[i+1]\{s_{i+1}\}}_{\alpha_i\alpha_{i+1}} \lambda^{[i+1]}_{\alpha_{i+1}} |\Psi^{[1\ldots i-1]}_{\alpha_{i-1}}\rangle|s_i\rangle|s_{i+1}\rangle|\Psi^{[i+2\ldots L]}_{\alpha_{i+1}}\rangle, \tag{2.11}$$

where the $\tilde{\Gamma}$s and $\tilde{\lambda}$ denote the new matrices and eigenvalues obtained from the Singular Value Decomposition. Knowing the formulation of the state, operations, and decompositions in TEBD, we are ready to take a look at how the method is applied in practice. The recipe for determining the ground state is as follows:

1. **Begin with an initial guess state.** Usually the guess state is chosen to be a simple product state. For example in a Fermi-Hubbard system with five lattice sites the initial state could be $|\emptyset\rangle_1|\uparrow\rangle_2|\uparrow\downarrow\rangle_3|\uparrow\rangle_4|\emptyset\rangle_5$. Such a non-entangled state in terms of λs and Γs means that in each lattice site the first term of the Schmidt decomposition is one ($\Lambda^{[i]}_1 = 1$) and all the other terms are zero ($\Lambda^{[i]}_\alpha = 0$, $\alpha \neq 1$). Moreover, all the Γs have only one nonzero element, ($\Gamma^{[i],\{s_i\}}_{11} = 1$, where $\{s_i\}$ for example at site $i = 0$ is $|\emptyset\rangle$).

2. **Operate by the operator $\mathbf{e^{-\tau \hat{H}_{FH}}}$**
   Remember that $|\Psi(t=0)\rangle = \lim_{\tau\to\infty} \frac{e^{-\tau \hat{H}_{FH}}|\Phi\rangle}{||e^{-\tau \hat{H}_{FH}}|\Phi\rangle||}$.

   The exponential needs to be divided into smaller segments as operating by the full $e^{-\tau \hat{H}_{FH}}$ would involve the exact diagonalisation of the whole system. Thus, the full Hamiltonian is separated into even and odd lattice sites $\hat{H}_{FH} = \hat{H}_{odd} + \hat{H}_{even}$ and the second approximation of TEBD is made, namely the Suzuki-Trotter expansion

$$e^{-\imath(\hat{H}_{odd}+\hat{H}_{even})\delta t} = e^{-\imath \hat{H}_{odd}\delta t} e^{-\imath \hat{H}_{even}\delta t} + O(\delta t)^2, \tag{2.12}$$

   where the error involved using the expansion scales with $(\delta t)^2$. Also higher order Suzuki-Trotter decompositions are possible, making the time step error scale as $(\delta t)^4$ or (δt^6) if needed. After having separated the even and odd terms one notices that now all the terms in $\hat{H}_{odd}$ commute with each other (similarly for $\hat{H}_{even}$). Thus, one can further segment the exponential, now without the Suzuki-Trotter error, and the operation simplifies into single on-site and nearest-neighbour operations described by Equations 2.8 and 2.11, respectively.

3. **Do step 2) until the ground state has been reached.** There are different convergence criteria one can use to determine that the ground state is reached. For example, the change of λs and Γs can be monitored and when their change is small enough one can deduce that the ground state has converged. We have compared TEBD ground states to the states obtained by the exact diagonalization with a low number of lattice sites and found out that the results are the same.

The time evolution follows almost the same recipe, with imaginary time replaced with real time, and the initial state for the time evolution is usually the state obtained from the ground state calculation. With this discussion we have compactly[1] gone through the main points of TEBD. Let us now look back and reflect on couple of the points.

The approximation done in the Schmidt truncation works well when, sorting the eigenvalues in descending order, the eigenvalues decay quickly. The decay of the eigenvalues is connected with the level of entanglement between the different lattice sites. In the case of low energy states of a

[1] We refer to [107, 110, 112] for more thorough and rigorous description.

1D system, the Schmidt coefficients decay approximately exponentially [107, 108, 110, 112] and χ can be truncated effectively. A way of measuring the entanglement between the different lattice sites of the system is the von Neumann entropy $S = Tr[\rho \log \rho]$, where ρ is the density matrix, and Tr denotes the trace. The entropy scales with available phase space [108] and as in 1D the phase space is the smallest, the entropy is smallest, and therefore the entanglement is low. Indeed, simulating higher dimensional systems with TEBD can be very challenging as in addition to the increased lattice site also higher χ would be required, based on the entropy argument.

Continuing on the approximations of TEBD, the error caused by the Suzuki-Trotter decomposition is controlled by reducing the time step. The means of monitoring whether the Schmidt truncation or the Suzuki-Trotter decomposition error affect the problem is that one calculates the same problem with larger χ and/or smaller time step δt and observes whether the results change. One can also look at the values of λ and see how they decay.

The TEBD computational time scales with χ^3 and L. As an example of the resource use, for a system with $S = 4$, $L = 150$ and $\chi = 150$, time-evolution of the system up to $t = 40\frac{1}{J}$ (time in the inverse units of the hopping element) takes 20 CPU hours and for the calculation 2 GB of soft memory is required. The ground state calculations are usually quicker, but they depend on how good is the guess for the ground state.

Finally, we have not explained how correlation functions can be calculated. We have developed a parallelised code for calculating the correlators, which speeds up the calculation significantly. Although the parallelisation will not be presented here, it is useful to show the recipe for simple and efficient calculation of the correlations next.

2.1.2 Calculating correlation functions

Following the scheme suggested by Andrew Daley [112], correlation functions of the form $C_{ij} = \langle \Psi | \hat{A}_i \hat{B}_j | \Psi \rangle$, where $\hat{A}_i$ and $\hat{B}_j$ are operators that act only on single sites i and j can be calculated recursively using four dimensional tensors G so that

$$G^i_{\alpha\beta} = \sum_{\gamma,\{\delta\}} {\lambda^i_\gamma}^2 \Gamma^{i\{X_i\}}_{\gamma\alpha} \Gamma^{i\{Y_i\}*}_{\gamma\beta} \tag{2.13}$$

$$
\begin{aligned}
G^{i+1}_{\alpha\beta} &= \sum_{a,b,\{\delta\}} G^{i}_{ab}\lambda^{i+1}_{a}\Gamma^{i+1\{\delta\}}_{a\alpha}\lambda^{i+1}_{b}\Gamma^{i+1\{\delta\}^*}_{b\beta} \\
&\cdots \\
G^{j-1}_{\alpha\beta} &= \sum_{a,b,\{\delta\}} G^{j-2}_{ab}\lambda^{j-1}_{a}\Gamma^{j-1\{\delta\}}_{a\alpha}\lambda^{j-1}_{b}\Gamma^{j-1\{\delta\}^*}_{b\beta} \\
G^{j}_{\alpha\beta} &= \sum_{a,b,\{\delta\}} G^{j-1}_{ab}\lambda^{j}_{a}\lambda^{j+1}_{\alpha}\Gamma^{j\{X_j\}}_{a\alpha}\lambda^{j}_{b}\Gamma^{j\{Y_j\}^*}_{b\beta}\lambda^{j+1}_{\beta},
\end{aligned}
$$

where i is the lattice site index, α, β and γ denote the Schmidt indices of λs and Γs, $\delta = \emptyset, \uparrow, \downarrow$ or $\uparrow\downarrow$ is the spin index, * denotes the complex conjugate, and X & Y represent the terms in the summation over spin indices that survive after operating with $\hat{A}_i$ or $\hat{B}_j$. For example if $\hat{A}_i = c^{\dagger}_{i\uparrow}$ then in the spin summation only terms with $Y_i = \emptyset, \downarrow$ and, correspondingly, $X_i = \uparrow, \uparrow\downarrow$ survive due to the orthogonality of spin states. The correlation function C_{ij} is obtained simply from $G^{j}_{\alpha\beta}$ by summing over the remaining indices

$$
C_{ij} = \langle\Psi|\hat{A}_i\hat{B}_j|\Psi\rangle = \sum_{\alpha\beta} G^{j}_{\alpha\beta}. \tag{2.14}
$$

The states outside the range $[i, j]$ do not contribute to the calculation as the Gs from 0 to $i-1$ are one due to the orthogonality. In the numerical implementation the calculation is sped up significantly by saving the obtained G^{j-1}s. To elaborate, after having calculated C_{ij} if one wants to calculate $C_{i(j+1)}$ then it is convenient to start from G^{j-1} in the recursive calculation with no need to repeat the earlier steps again.

We have now gone compactly through the implementation of TEBD, and described a recipe for efficient calculation of correlation functions using the method. Let us finally note that being able to calculate correlation functions from the information about the state (λs and Γs) is an advantage, useful particularly in the study of superfluid systems. This finishes off our discussion on TEBD which is the numerical method that has been used in obtaining results in Publications I-V. Next we will move away from numerics, and explore an analytical method that can be applied in the research of ultracold gases.

2.2 The Kadanoff-Baym formalism

Developed by Gordon Baym and Leo Kadanoff in 1961 [113, 114], the Kadanoff-Baym formalism is a many-body theory used for calculating the response of a system to an external perturbation. Understanding the response of the system to perturbations is important, because it tells us

valuable information of the state, e.g. whether the system is superfluid. The idea of the Kadanoff-Baym method is simply that we will obtain a better approximation for the response by requiring that the conservation laws present are satisfied. However, in order to understand how the method works, we need to discuss the background of the problem first.

2.2.1 The linear response

The basic problem is that there is a many-body system described by a wave-function $\Psi(\mathbf{r}, t)$. Then one applies a perturbation $P(\mathbf{r}, t)$ on the system and asks how the system changes in response to the perturbation. If the function describing the response $\chi(\mathbf{r}, t, P)$ is found, one can predict how the system changes when for example subjected to radio frequency radiation or shot with a laser. Importantly, some of the changes can be specific to the state of the system, revealing e.g. antiferromagnetic order. When the perturbation is small ($P \rightarrow 0$) only the term first order in P contributes, and the function $\chi(\mathbf{r}, t)$ (which no longer has explicit dependence on P) becomes the linear response function. The state of the system $\Phi(\mathbf{r}, t)$ in the theory of linear response is given by

$$\Phi(\mathbf{r}, t) \approx \Psi(\mathbf{r}, t) + \int_{-\infty}^{t} \chi(\mathbf{r}, t^{'})\Psi(\mathbf{r}, t^{'})dt^{'}. \tag{2.15}$$

Equation 2.15 approximates that the state of the system Ψ does not change significantly during the time that the perturbation is applied, and therefore the final state Φ represents the weighted sum of all events that have occurred in the system in the past when it was approximately in the state Ψ. Being interested in determining the linear response function, let us next look at how that can be done.

2.2.2 Determining the linear response function

Here we start off by outlining the building blocks of many-body linear response theories, described extensively in e.g. [115]. Instead of wave-functions one works with Green's functions and self-energies. We will first go through what these quantities mean and how is the linear response function determined in such a picture. The linear response function χ_G to a perturbation P is obtained from the Green's function $\mathbf{G}$ by

$$\chi_G \approx \frac{\delta G}{\delta P}, \tag{2.16}$$

when $\delta P \to 0$. The Green's function describes physically the probability of a single particle propagating from one state to another. It is in general obtained from the Dyson's equation

$$G = \frac{G_0}{1 - G_0\Sigma}, \tag{2.17}$$

where Σ is the self-energy, $G_0(k,\omega) = \frac{-1}{E(k)-\imath\omega}$ is the free particle Green's function (which describes a probability of a free particle propagating from one state to another, without the effect of other particles in the full many-body system), $E(k)$ is the free particle dispersion relation, and w is the frequency. Formulating the problem in this manner all the troublesome physics has been effectively put into the self-energy Σ. The self-energy can be intuitively understood to mean the change in energy (or mass) of a particle, when compared to the single free particle, as a result of interactions with the other particles of the system.

The self-energy Σ cannot be usually written out without approximations and this is where many-body theories can deviate from each other by selecting a different approximation scheme for the self-energy. The choice of Σ can be problematic, and approximations done can lead to problems that need to be corrected later (c.f. delta function potential and regularisation of the gap equation in the continuum BCS). For example, it may turn out that the obtained χ_G breaks the conservation laws of the system. This brings us to the Kadanoff-Baym method. It provides a recipe for enforcing χ_G to obey the conservation laws present in the system regardless of the approximation done for Σ.

Now, the way to make the χ_G to obey the conservation laws is that one starts from the equation of motion[2] for the Green's function which has the conservation laws embedded (see [113] for the proof)

$$\mathbf{G^{-1}} = \mathbf{G_0^{-1}} - P\tau - \mathbf{\Sigma}, \tag{2.18}$$

where τ is a matrix describing what states are coupled by the perturbation P. In Equation 2.18 G, Σ and G_0 have been written in the matrix form so that the Green's function describing the single particle propagation from state $\Psi_a(\mathbf{r}, t)$ to state $\Psi_b(\mathbf{r}', t')$ is given by

$$G_{ab}(\mathbf{r}, t, \mathbf{r}', t') = -\imath\langle T\Psi_a(\mathbf{r}, t)\Psi_b^\dagger(\mathbf{r}', t')\rangle, \tag{2.19}$$

where T is the time-ordering operator and $\imath$ is the imaginary unit. Now,

[2] We have dropped the integrals in the e.o.m. for clarity.

$$\begin{aligned} \mathbf{G}\mathbf{G}^{-1}\mathbf{G} &= \mathbf{G} && (2.20)\\ \Rightarrow \frac{\delta \mathbf{G}}{\delta P} &= \frac{\delta \mathbf{G}}{\delta P}\mathbf{G}^{-1}\mathbf{G} + \mathbf{G}\frac{\delta \mathbf{G}^{-1}}{\delta P}\mathbf{G} + \mathbf{G}\mathbf{G}^{-1}\frac{\delta \mathbf{G}}{\delta P} && (2.21)\\ \Rightarrow \frac{\delta \mathbf{G}}{\delta P} &= -\mathbf{G}\frac{\delta \mathbf{G}^{-1}}{\delta P}\mathbf{G}. && (2.22) \end{aligned}$$

But

$$\frac{\delta \mathbf{G}^{-1}}{\delta P} = -\tau - \frac{\delta \mathbf{\Sigma}}{\delta P} \tag{2.23}$$

and hence

$$\frac{\delta \mathbf{G}}{\delta P} = \mathbf{G}(\tau + \frac{\delta \mathbf{\Sigma}}{\delta P})\mathbf{G}. \tag{2.24}$$

Substituting this into Equation 2.16 one obtains

$$\chi_{\mathbf{G}} \approx \mathbf{G}(\tau + \frac{\delta \mathbf{\Sigma}}{\delta P})\mathbf{G}, \tag{2.25}$$

which is the final result. When Equation 2.25 is used for determining χ_G it has been made sure that the conservation laws are satisfied. This is the idea of Kadanoff-Baym method which have been used to derive results in Publications I and II. Having finally covered most the physics required to understand the publications presented in this thesis we move on to discuss about the interesting results.

3. Results

3.1 Radio-frequency spectroscopy for superfluid Fermi gases

We start off the analysis of the results of Publications I-V by looking at the radio frequency (rf) spectrum of a superfluid one-dimensional Fermi gas in a lattice. In Publication I we ask what happens when one of the spin components forming the superfluid is transferred to a third spin state, as shown in Figure 3.1. The aim of the work is to learn about the nature of the 1D superfluid as well as the nature of the radio frequency transfer process. In particular, we include in our analysis the interactions between the final state (f) and state $\uparrow$ (see Figure 3.1) [116, 117, 118]. The rf-spectrum is obtained using TEBD, and the results of the TEBD time evolution are compared to the results of the Kadanoff-Baym analytics with the BCS approximation for the self energy.

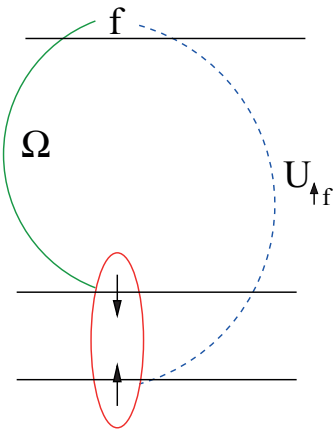

Figure 3.1. Spin up and down particles form a superfluid, and the system is perturbed by rf-radiation transferring a particle from down state to the final state f. The final state interaction with the up state is included in the analysis.

The energy of the rf-radiation must overcome the pairing energy of the superfluid state for the transfer to occur. Therefore the peak of the rf-spectrum for the superfluid will shift compared to the rf-peak of the non-interacting state. To describe this conveniently a parameter called detuning $\delta = \omega_{RF} - \omega_{free}$ is introduced, where ω_{free} is the position of the transition peak for the non-interacting state, and ω_{RF} is the frequency of the rf-radiation. Now, the system is described by the Fermi-Hubbard Hamiltonian with radio frequency coupling Ω between states $\downarrow$ and f

$$\begin{aligned} H &= -J \sum_{i,\sigma=\uparrow,\downarrow,f} c^\dagger_{i\sigma} c_{i+1\sigma} + H.c. \\ &\quad -U_{\uparrow\downarrow} \sum_i \hat{n}_{i\uparrow}\hat{n}_{i\downarrow} - U_{\downarrow f} \sum_i \hat{n}_{i\uparrow}\hat{n}_{if} \\ &\quad + \sum_i \frac{\delta}{2}(c^\dagger_{i\downarrow} c_{i\downarrow} - c^\dagger_{if} c_{if}) \\ &\quad + \Omega \sum_i (c^\dagger_{if} c_{i\downarrow} + c^\dagger_{i\downarrow} c_{if}), \end{aligned} \tag{3.1}$$

where the final state interactions between $\uparrow$ and f are included but the final state interactions between $\downarrow$ and f are neglected as these do not shift the rf-peak by symmetry arguments (rf-coupling being SU(2) invariant, see [116]).

We calculate the ground state with TEBD, with $\delta = 0$, $\Omega = 0$, and forcing $n_f = 0$. The up and down components form a balanced ($n_\uparrow = n_\downarrow$) superfluid in the ground state. The time evolution of the system in response to the rf pulse is calculated using TEBD time evolution, and as results we obtain the rf-spectra and the detunings describing the rf-shift shown in Figures 1-3 in Publication I.

Moving on to discuss the results, sum rule considerations with Kadanoff-Baym formalism and the BCS approximation for the self-energy predict that the average shift of the rf-peak is given by [116]:

$$\bar{\delta} = (U_{\uparrow f} - U_{\uparrow\downarrow}) \left(n_\uparrow + \frac{\Delta^2}{U^2_{\uparrow\downarrow} n_\downarrow} \right), \tag{3.2}$$

where Δ is the BCS gap. Based on the results presented in Figures 1-3 of Publication I, we find that for short times the Kadanoff-Baym + BCS result is in good accordance with the spectral shift from TEBD numerics, but for longer times the result starts to break down, the disparity between the numerics and Equation 3.2 becoming higher with increasing $U_{\uparrow\downarrow}$ and $U_{\uparrow f}$ (see Figures 1-2 in Publication I). In fact, the spectra presented in

Figure 3 are all short time spectra ($t = 0.8\Omega^{-1}$) and the long time spectra have different qualitative features. What happens is that at longer times the spectrum is not symmetric, as it is often the case with systems that have non-trivial structure in the density of states. The average position of the whole spectrum is at all times consistent with Equation 3.2 and the disparity we see in Figures 1-2 is caused by the fact that the non-trivial shape of the spectrum starts to develop but at the short times presented in Figure 3 we do not see it yet.

Moreover, the effect of the final state interactions [116] on the position of the rf-peak are significant also in the 1D lattice system, verified by our results shown in Figure 2 of Publication I. Having described the main results of Publication I let us now move on to the physics of the asymmetric Josephson effect.

3.2 Is the Josephson effect really about coherent tunnelling of Cooper pairs?

As discussed above, ultracold atomic gases provide a means of exploring novel and exotic physics. A prime example of such an exotic system is a gas in which one can effectively create different voltages for spin up and down components across a Josephson junction [119]. The physics of this kind of asymmetric Josephson junction is explored in Publication II. The asymmetric junction can be created using for example spin dependent potentials, which is depicted in Figure 3.2. Looking at Figure 3.2 we see that there are two superfluids in separate wells, and the voltage difference across the wells comes from the potential drop being less for the up component than the down component.

In Publication II we calculate the current between the wells as a response to the perturbation caused by the asymmetric double well potential (Ω) using the Kadanoff-Baym formalism. Intuitively one might expect that the Josephson current between the two wells has the same amplitude of up and down particles, as the Cooper pairs tunnel together across the barrier in the Josephson effect. However, we find that the amplitude of spin up and spin down Josephson oscillations is different, contrary to the intuition. This sounds quite interesting so let us elaborate on the work done. The Hamiltonian of the system shown in Figure 3.2 is

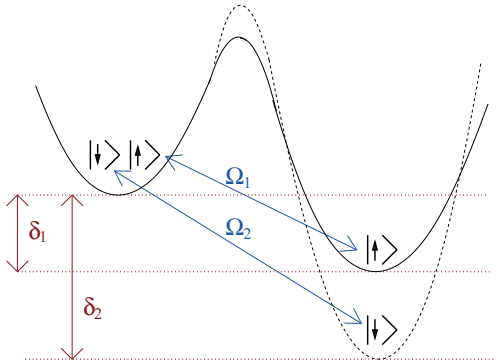

Figure 3.2. A superfluid composed of spin up and down particles in a spin-dependent double well. Ωs describe the tunnelling coupling and δs the potential difference between the wells which is analogous to voltage.

$$
\begin{aligned}
H = \quad & H_0 + H_T && (3.3)\\
H_0 = \quad & \int d\,\mathbf{r} \sum_i \psi_i^\dagger(\mathbf{r}) \left(-\frac{\nabla^2}{2m} - \mu_i \right) \psi_i(\mathbf{r}) && (3.4)\\
& + \frac{1}{2} \int d\,\mathbf{r} \sum_{i \neq j} U_{ij} \psi_i^\dagger(\mathbf{r}) \psi_j^\dagger(\mathbf{r}) \psi_j(\mathbf{r}) \psi_i(\mathbf{r}) \\
H_T = \quad & \frac{\delta_1}{2} \int d\,\mathbf{r} (\psi_1^\dagger(\mathbf{r}) \psi_1(\mathbf{r}) - \psi_3^\dagger(\mathbf{r}) \psi_3(\mathbf{r})) && (3.5)\\
& + \frac{\delta_2}{2} \int d\,\mathbf{r} (\psi_2^\dagger(\mathbf{r}) \psi_2(\mathbf{r}) - \psi_4^\dagger(\mathbf{r}) \psi_4(\mathbf{r})) \\
& + \Omega_1 \int d\,\mathbf{r}\, \psi_1^\dagger(\mathbf{r}) \psi_3(\mathbf{r}) + h.c. \\
& + \Omega_2 \int d\,\mathbf{r}\, \psi_2^\dagger(\mathbf{r}) \psi_4(\mathbf{r}) + h.c.,
\end{aligned}
$$

where $\psi_i(\mathbf{r})$ and $\psi_i^\dagger(\mathbf{r})$ are the fermionic field operators (in continuum) annihilating and creating a state i, respectively, where $i = 1$ represents up particle in the left well, $i = 2$ down particle in the left well, $i = 3$ up particle in the right well, and $i = 4$ down particle in the right well, μ_i is the chemical potential, and U_{ij} are the interaction strengths having assumed a delta function potential $U_{ij} = V_{ij}\delta(r - r')$ and integrated out the r' degree of freedom. We assume that U_{12} and U_{34} lead to BCS type of pairing. Across-the-well interactions like U_{14} can be neglected. Ω represents the coupling and δ the potential difference between the wells.

Calculating the Josephson currents using the Kadanoff-Baym formalism with the BCS approximation for the self-energy we obtain:

$$
I_\uparrow^J(t) \quad = I_\uparrow^C(\delta_2) \sin[(\delta_1 + \delta_2)t] \qquad (3.6)
$$

$$I^J_\downarrow(t) \quad = I^C_\downarrow(\delta_1)\sin[(\delta_1+\delta_2)t], \tag{3.7}$$

where $I^J_\uparrow$ denotes the Josephson current of up particle from left well to the right well (note that $I^J_\uparrow$ and $I^J_\downarrow$ would be equal if the potentials for spin up and down would be the same), and the amplitudes I^C are given by

$$I^C_\uparrow(\delta_2) = \quad 2\left|\Omega_1\Omega_2\Pi_{\mathcal{F}}(\mathbf{p}=0,\delta_2+i\eta^+)\right| \tag{3.8}$$

$$I^C_\downarrow(\delta_1) = \quad 2\left|\Omega_1\Omega_2\Pi_{\mathcal{F}}(\mathbf{p}=0,\delta_1+i\eta^+)\right|, \tag{3.9}$$

where

$$\Pi_{\mathcal{F}}(\mathbf{p},\omega) = \frac{1}{\beta V}\sum_{\mathbf{q},\gamma}\mathcal{F}_{12}(\mathbf{q},\gamma)\mathcal{F}^*_{34}(\mathbf{q}-\mathbf{p},\gamma-\omega), \tag{3.10}$$

Fs are the anomalous BCS Green's functions coming from the BCS approximation for self energy and Equation 3.10 comes from applying Equation 2.25. Note that compared to Equation 2.25 Fs have been Fourier transformed to momentum and frequency space ($\mathbf{p}$, ω). Furthermore, V is the volume, $\beta = 1/(k_BT)$, T is temperature, and k_B is the Boltzmann constant. The details of the Kadanoff-Baym calculation are presented in the supplementary material of Publication II.

The important thing to notice in our result, Equations 3.8 and 3.9, is that the amplitude of up component oscillations depends on δ_2, whereas the amplitude of down component oscillations depends on δ_1. Having these two different from each will therefore result in oscillations with a different amplitude. Numerically solving Equations 3.6 and 3.7 confirms this, see Figure 3.3. Thus we have arrived at the result that in the presence of the asymmetric potentials (i.e. different voltages) the constituents of Cooper pairs oscillate at different amplitudes. We call this phenomenon the asymmetric Josephson effect.

But why is this so? Should not the Cooper pairs tunnel together? Intuitive physics is somewhat lost in the many-body formalism and we would like to understand the reason for the asymmetry. The clue for the physical origin of the effect comes from two sources. Firstly, we have solved the dynamics of the system also using time-dependent perturbation theory to the second order in the rf-couplings. Secondly, we have used exact diagonalisation to solve the time evolution of a small system comparable to the double well set-up considered here. We refer the intrigued reader to Publication II for the proof and present here only the result of the analysis.

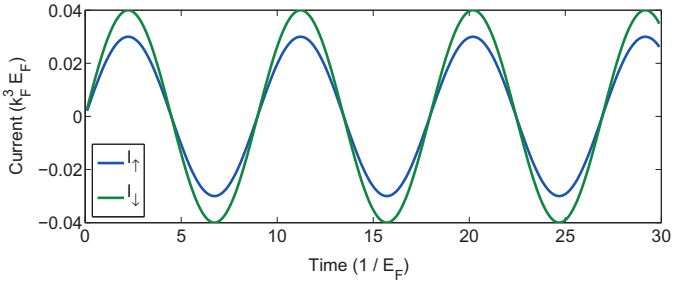

Figure 3.3. The obtained spin up and down Josephson oscillations across the barrier, with $\Omega_1 = \Omega_2 = 1.0$, the BCS gap $\frac{\Delta}{E_F} = 0.24$, the chemical potential $\frac{\mu}{E_F} = 0.94$ (Δ and μ chosen to be the same for the both sides of the well), $\frac{\delta_1}{E_F} = 0.3$, $\frac{\delta_2}{E_F} = 0.4$, and E_F is the Fermi energy.

By comparing the Kadanoff-Baym results (Equations 3.8 and 3.9) to the perturbation theory and exact diagonalisation analysis it turns out that the asymmetry is caused by the interference of the broken pair states, as portrayed in Figure 3a of Publication II. Broken pair states are virtual (intermediate) states in which e.g. up particle has tunnelled over the barrier, but the down particle it is paired with has not. At zero temperature the broken pair states are energetically forbidden since the energy to enter them costs 2Δ. However, the virtual tunnelling via these states causes the asymmetry in the current. In the symmetric (usual) Josephson effect this phenomenon is not visible since, although the broken pair interference term is present, the contributions from the broken pair states are the same for both of the spins. Nonetheless, our work suggests that the interference term should also be included to the description of the symmetric Josephson effect.

Summing up, we have predicted and explained a new phenomenon: the spin-asymmetric Josephson effect. In the effect spin up and down components oscillate at the Josephson frequency with different amplitudes across the junction. This suggests that the traditional interpretation of the Josephson effect as coherent tunnelling of Cooper pairs needs to be modified in the light of the existence of the broken pair interference term.

3.3 The expansion of a band-insulator state

In Publication III we have investigated what happens if a one-dimensional band insulator state is released to expand into the surrounding empty

lattice. To elaborate, initially there is a state as shown in Figure 3.4, i.e. pairs in the middle and empty lattice sites on the outside. The setup is the same as in the experiment with a two dimensional lattice by [121]. Experimentally the expansion is realised by having initially such a deep lattice that the pairs localise on the lattice sites, and to initiate the expansion the lattice depth is suddenly lowered.

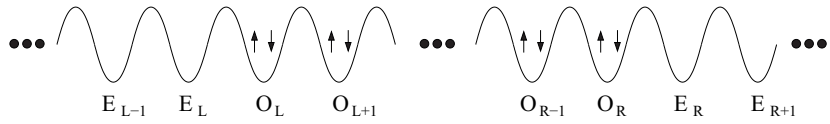

Figure 3.4. Schematic representation of the initial state: the middle part of the lattice is fully occupied (O_i) and the rest is empty (E_i). Sites E_L, O_L and O_R, E_R represent the left and right edge of the cloud, respectively.

We have simulated the expansion using TEBD with the Fermi-Hubbard Hamiltonian. The ground state has been input to the algorithm manually, as the initially localised pairs are described by an easy product state. From the TEBD time evolution, we have obtained as results the density profiles of up particles $n_\uparrow(t)$, down particles $n_\downarrow(t)$ and doublons[1] $n_{\uparrow\downarrow}(t)$ which represent doubly occupied sites $c_\uparrow^\dagger c_\downarrow^\dagger|\emptyset\rangle$.

For convenience, we present the figures depicting the main results of Publication III here as well. Figure 3.5 shows the obtained up particle and doublon density profiles, respectively, in the case of the strong attractive interaction $U = -10J$. The problem is up $\leftrightarrow$ down symmetric so the down particle density is not shown. Figure 3.6 shows the the density of unpaired up particles $n_{\uparrow\downarrow}(t) - n_\uparrow(t)$ zoomed in at the initial cloud position.

To understand the physics behind the expansion we have analysed the numerical results in the light of the two-site model as presented in Section 1.3.3. Initially, all the particles are paired. The central lattice sites are Pauli blocked so the dynamics must initiate from the edges of the cloud. Indeed, what we see in Figure 3.6 is the formation of unpaired particles at the edges, with a characteristic oscillation frequency. We suggest that in the strong interaction limit the edge dynamics is explained by considering the two-site physics between the sites $O_L\&E_L$ and $O_R\&E_R$ as defined in Figure 3.4.

[1]For the reader it might seem that a more natural definition for a 'doublon' is simply a 'pair'. However, whereas a doublon is certainly a localised pair, other kind of pairs also exist. For example in BCS the pairs are not localised in position space. Hence, to distinguish the nature of the pair as localised in position space we use the term 'doublon'.

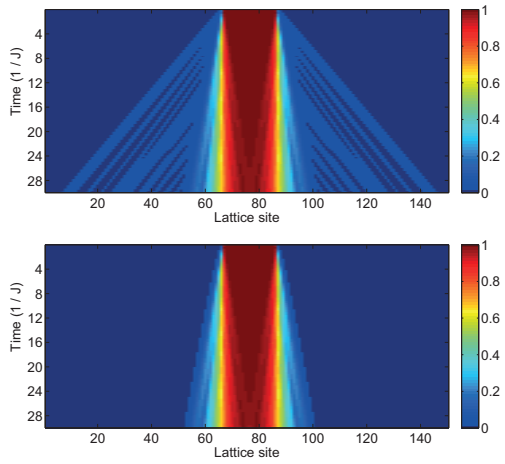

Figure 3.5. Time evolution of $\sqrt{n_{i\uparrow}(t)}$ (above) and $\sqrt{n_{i\uparrow\downarrow}(t)}$ (below) for $U = -10.0J$. We are plotting the square roots of the density in order to enhance the low density features important for the analysis.

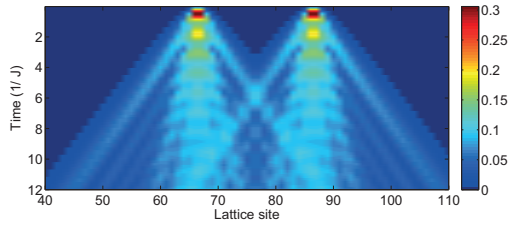

Figure 3.6. Unpaired particle expansion $n^{un}_{i\uparrow}(t) = n_{\uparrow\downarrow}(t) - n_{\uparrow}(t)$ for $U = -5.0J$.

The observed oscillation frequency and the amplitude of unpaired particles produced at the edge are compared to the predictions of the two-site model. From Equation 1.22 the frequency and the amplitude are given by $\sqrt{U^2 + 16J^2}$ and $\frac{8}{16+\frac{U^2}{J^2}}$, respectively. The comparison is presented in Figures 6-7 of Publication III. Furthermore, the decay of the amplitude of these oscillations can be calculated using the two-site model as well. The results of this calculation are compared to the TEBD data in Figure 8 of Publication III. Summing up the analysis reveals that the dynamics of the problem is indeed explained by the simple two-site model. In other words, the doublon $\leftrightarrow$ singlet conversion occurs via the Hubbard Dimer mechanism taking place at the cloud edge, as in the strong interaction limit the two-site process at the edge dominates over higher order processes.

What is more, we see in Figure 3.5 that there are two ballistic expansion fronts originating from the edge of the initial cloud. The outermost

front is made of unpaired particles, whereas the innermost front is fully paired. The two expand with constant velocities, i.e. the slopes of the expansion seen in Figure 3.5 is constant. Next, we proceed to elucidate what determines the velocities of the propagation.

The group velocity of the free (unpaired) particles in lattice is $v_g = \frac{dE}{dk} = 2J\sin(k)$ since the lattice dispersion is $1 - 2J\cos(k)$. Hypothesising that the expansion velocity is given by the group velocity we expect therefore that the velocity reflects the momentum distribution of the ground state. In a band insulator we have a flat momentum distribution due to initially localised pairs (described by an array of delta functions in position space). Thus the maximum and average group velocities are obtained when $k = \frac{\pi}{2}$. Hence the predicted velocity for the unpaired particles is $2J$. Looking at the outermost (unpaired) wavefronts in Figure 3.5, the results of TEBD numerics are in excellent accordance with this result.

Regarding the doublons, it can be shown that the doublon hopping corresponds to the hopping of a non-interacting particle with $J_{eff} = \frac{4J^2}{U}$ [95, 120]. Consequently, we expect that the innermost wavefronts expand with velocity $\frac{4J^2}{U}$, which we also find to be in perfect agreement with the TEBD results. Since the two wavefronts are ballistic, i.e. the expansion can be described by the expansion of non-interacting particles with renormalised J for doublons, we are led to postulate that the expansion physics is characterised by a two-fluid picture. In the two-fluid picture the doublons and unpaired particles are separate fluids which do not interact with each other, except at the cloud core. Only in the cloud core the density is high enough for the interaction between the fluids to occur. But the deep core is Pauli blocked due to density of both spin components being one. Hence the conversion between doublons and unpaired particles happens dominantly at the edges of the core. And, it is restated that the conversion mechanism at the edges comes from the simple two-site physics. Note also the hole expansion fronts moving into the core of the cloud in Figure 3.5. The hole wavefronts are symmetric to particle wavefronts and are also explained by two-site dynamics. Finally, it is pointed out that the two-fluid model is supported by analytical Bethe Ansatz considerations in 1D continuum [106].

Using the density profiles we have determined the expansion velocity of the gas cloud, and compared our results to the experiment [121] with the 2D lattice. Comparing Figure 5 of [121][2] and Figure 5 in Publication III

[2]The results of [121] have not been yet published at the time of the writing and

we observe that although the experiment is in 2D and at finite temperature the experimental results match the results of the TEBD numerics well.

Before summarising, let us note that we have shown only the strongly interacting $\frac{|U|}{J} > 3$ results here. For middle interactions $0.5 < |\frac{U}{J}| < 3$ the core becomes quickly Pauli unblocked, and the number of sites that contribute to the dynamics increase. To determine the total time development of the system in such a case one should consider the interference between all different sites, and this in fact is something that we have considered in Publication IV, although in a different context. For low interactions $|\frac{U}{J}| < 0.5$ the system behaves like a non-interacting system, everything expanding at speed $2J$. Another interesting point that we have not discussed yet is that we observed $U \leftrightarrow -U$ symmetry in the TEBD expansion data. The time development of density profiles is exactly the same for all $U \leftrightarrow -U$ simulated. This feature is in accordance with the general time-dependent properties of the Fermi-Hubbard model. Finally, it is intriguing that the 2D experimental results are so alike to our 1D simulations. But perhaps it does not come as a surprise. After all, the Hubbard Dimer analysis should carry on to higher dimensions as if one considers 2D the core is again Pauli blocked and the two-site mechanism takes place at the edges of the square. Considering only the direction perpendicular to the edges, an assumption valid in the first order, the analysis simplifies into the 1D model.

To summarise, in Publication III we have shown that the expansion of the band insulator state is explained by a two-fluid model, the two fluids being the doublons and unpaired particles. The interaction between the two fluids is determined by the two-site Hubbard model dynamics. The results of our 1D TEBD simulations are very similar to the 2D experimental results [121], both showing the $U \leftrightarrow -U$ symmetry and the core expansion speed determined by the two-fluid Hubbard Dimer picture.

3.4 The collision of spin-polarized gases

In Publication IV we look at the physics of the collision of oppositely spin polarised gases. The schematic of the system considered is shown in Figure 3.7. Initially we have two spin-dependent harmonic traps that sepa-

thus we do not have the permission for reprinting them here.

rate the up and down spin components, and at time zero we release the harmonic traps, allowing the gases to expand and collide. We employ TEBD and the Fermi-Hubbard Hamiltonian with harmonic trapping to describe the physics of the problem, and obtain the density profiles $n_{\uparrow}(t)$, $n_{\downarrow}(t)$, and $n_{\uparrow\downarrow}(t)$ as the results of the simulation. Our setup is similar to the experiment by [122], the differences being that we have a lattice and consider 1D, whereas the experiment is in continuum and is not restricted to 1D. However, we expect similarity with the experiment as the Fermi-Hubbard model maps to the continuum Gaudin-Yang model in the strongly interacting, low density limit [98, 120], and we observed that 1D TEBD results match the results of 2D experiment [121] in the band insulator case.

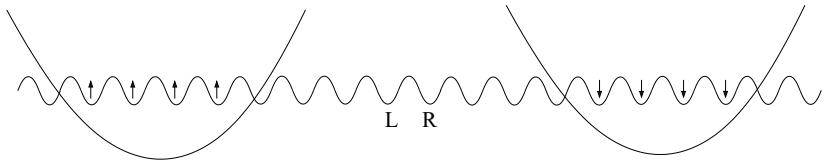

Figure 3.7. The system. Spin up and down gases in a lattice are confined in two separate harmonic potentials. At time zero the harmonic potentials are removed and the gases expand and collide. Here, L and R mark the two central sites where the expanding gases meet.

We suggest in Publication IV that the collision dynamics is determined by an extension of the two-site Hubbard Dimer model which was discussed in the first chapter. Initially when the gases come into contact, there is doublon population at only the two central lattice sites. When the collision progresses, more particles enter the central sites, and the number of sites which have nonzero doublon population increases. We propose that at each of the lattice sites with nonzero doublon population the unpaired particle to doublon conversion occurs via the Hubbard Dimer mechanism. The aim is at formulating equations that describe the number of doublons produced in the collision, as this is of experimental interest and we might learn something from the qualitative dynamics by doing so. We will now follow the analysis also presented in Publication IV to derive the total number of doublons produced in the collision.

Let us define reaction center R as all the lattice sites which have nonzero population of both up and down particles. Moreover, we define the reaction edge sites $Edge(t)$ to mean the last sites that have both up and down particles, when counting from the center of the collision. The positions of

these edge sites change as a function of time as the collision progresses. Now, unpaired particles will tunnel into the reaction center from the sites which are adjacent to the edge sites. The density of unpaired particles in these sites is denoted $n_{un}^{N}(t)$. However, we need to take into account also unpaired particles tunnelling out of the reaction center. They tunnel out from the edge sites, at which the density is $n_{un}^{Edge}(t)$. Finally, in determining the total density of unpaired particles in the reaction center, we must consider that the unpaired particles will convert into doublons via Dimer dynamics. Summing up these contributions, we obtain for the total density of unpaired particles in the reaction center (R)

$$\tilde{n}_{un}^{R}(t) = 2(\sin(Jt))^2 n_{un}^{N}(t) - 2(\sin(Jt))^2 n_{un}^{Edge}(t) - \tilde{n}_{\uparrow\downarrow}^{R}(t), \tag{3.11}$$

where $\tilde{n}_{\uparrow\downarrow}^{R}(t)$ is the total number of doublons and the $2(\sin(Jt))^2$ term comes from solving the time-dependent problem of $|\emptyset,\uparrow\rangle$ converting into $|\uparrow,\emptyset\rangle$[3] in a similar fashion as the doublon $\leftrightarrow$ unpaired particle conversion has been solved in Section 1.3.3. Restating, the first term accounts for unpaired particles entering the reaction center, the second term accounts for unpaired particles leaving the reaction center and the last term accounts for unpaired particles converted into doublons (and vice versa). Next we consider the doublons. With the definitions above, we hypothesise that the growth (G) and decay (D) of $\tilde{n}_{\uparrow\downarrow}^{R}(t)$ are given by

$$G(t) = \int_{\tau=0}^{\tau=t} \int_{t'=\tau}^{t'=t} \frac{8}{16 + \frac{U^2}{J^2}} \tag{3.12}$$
$$(1 - \cos(\sqrt{U^2 + 16J^2}(\tau - t'))\tilde{n}_{un}^{R}(t')dt'd\tau,$$

$$D(t) = \int_{\tau=0}^{\tau=t} \int_{t'=\tau}^{t'=t} \frac{8}{16 + \frac{U^2}{J^2}} \tag{3.13}$$
$$(1 - \cos(\sqrt{U^2 + 16J^2}(\tau - t'))\tilde{n}_{\uparrow\downarrow}^{R}(t')dt'd\tau,$$

and the total number of doublons is

$$\tilde{n}_{\uparrow\downarrow}^{R}(t) = G(t) - D(t). \tag{3.14}$$

Equations 3.12 - 3.14 could be solved self-consistently to obtain the full time evolution predicted by the model (given the size and shape of the

[3]Note that this solution is another way of showing that the speed of the non-interacting expansion is $2J$.

incoming polarised clouds, i.e. $n^N_{un}(t)$), but let us instead see if one learns something from these equations by considering the high-interaction limit. In the high-interaction limit, we note that the cosine oscillations occur at such a high frequency that they will average out in the τ integration. Moreover, in the high interaction limit $|U| > 3$, $\tilde{n}^R_{\uparrow\downarrow}(t)$ which is present in the decay term in Equation 3.13 is negligible during the time of the collision, because the Hubbard Dimer pre-factor $\frac{8}{16+\frac{U^2}{J^2}}$ makes the density or doublons produced much less than the number of unpaired particles entering the reaction center from the expanding polarised clouds. Thus, substituting $G(t)$ into Equation 3.14 and neglecting the cosine term and $D(t)$ we have

$$\tilde{n}^R_{\uparrow\downarrow}(t) = \int_{\tau=0}^{\tau=t} \int_{t'=\tau}^{t'=t} \frac{8}{16+\frac{U^2}{J^2}} \tilde{n}^R_{un}(t')dt'd\tau. \tag{3.15}$$

Now, substituting in $\tilde{n}^R_{un}(t')$ from Equation 3.11 and again neglecting the $\tilde{n}^R_{\uparrow\downarrow}(t)$ term we obtain

$$\tilde{n}^R_{\uparrow\downarrow}(t) = \int_{\tau=0}^{\tau=t} \int_{t'=\tau}^{t'=t} \frac{8}{16+\frac{U^2}{J^2}}[2(\sin(Jt'))^2 n^N_{un}(t') \tag{3.16}$$

$$-2(\sin(Jt'))^2 n^{Edge}_{un}(t')]dt'd\tau, \tag{3.17}$$

which is our final result. Before proceeding to analyse the numerical data in the light of this result let us briefly reflect on where do the features of Equation 3.16 come from. The pre-factor $\frac{8}{16+\frac{U^2}{J^2}}$ is inherited from the two-site model. However, the oscillation frequency of the two-site model is no longer present. This is due to the fact that, in the high interaction limit, the $\sqrt{U^2+16J^2}$-oscillations are fast compared to the time scale of the collision so that they will average out in the τ integration. Therefore, the only oscillating term that is left in Equation 3.16 originates from the unpaired particle tunnelling in Equation 3.11.

The most important insight we obtain from Equation 3.16 is that we expect that the number of doublons produced to be proportional to the Hubbard Dimer amplitude $\frac{8}{16+\frac{U^2}{J^2}}$. Comparing the total number of doublons produced in TEBD simulation to $a\frac{8}{16+\frac{U^2}{J^2}}$, where a is the constant of proportionality, we find in the strong interaction limit the excellent fit shown in Figure 3.8.

The above analysis provides us insight in the qualitative dynamics of the problem. When $|U|$ becomes large we expect that the amplitude of

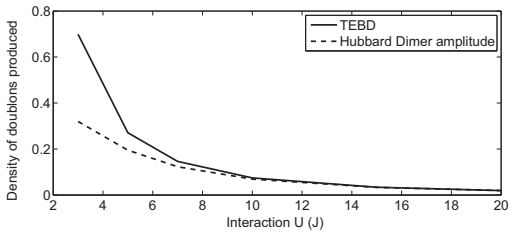

Figure 3.8. The total number of doublons produced obtained from TEBD numerics fitted to $a\frac{8}{16+\frac{U^2}{J^2}}$.

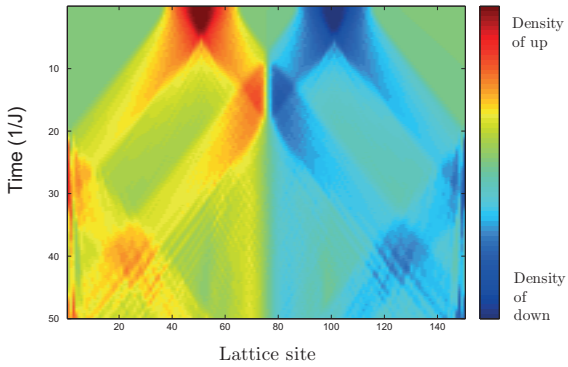

Figure 3.9. The density profiles of up $n_\uparrow(t)$ and down $n_\downarrow(t)$ particles for $\frac{|U|}{J} = 10.0$. We see that the colliding gases bounce back from each other.

doublon creation is low, and being unable to create doublons, the gases will bounce back from each other conserving the momentum in the collision. The TEBD results in Figure 3.9 show that in the strong interaction limit this indeed is the case. The gases bounce back from each other and, again, we find that there is $U \Leftrightarrow -U$ symmetry in the collision due to the U term being squared in the Hubbard Dimer formula. The interaction symmetry is actually quite intriguing and perhaps initially unintuitive. One might expect that attractively interacting gases will stick together, and repulsive gases bounce back. Nonetheless, this is not the case[4] due to the $U \Leftrightarrow -U$ symmetry present in the Fermi-Hubbard dynamics.

The experimental results by [122] are consistent with our results. In the experiment it was observed that the gases bounce back from each other with diffusivity being lower with higher interactions, and there is

[4]Another way of understanding the bouncing back is saying that the maximum energy for transition possible in the single band Hubbard model is $4J$. Thus when $|U| > 4J$ pair formation is out of resonance, and only unpaired particle - pair oscillations can happen, but with a suppressed amplitude for the pairs.

the $U \Leftrightarrow -U$ symmetry.

In summary we have extended the two-fluid Hubbard Dimer analysis originating from Publication III to explain the number of doublons produced in the collision of spin polarised one-dimensional gases, and thus the dynamics of the problem. Our results are in qualitative accordance with the experimental findings of [122].

3.5 Detecting the FFLO state in a time-of-flight measurement

As discussed in chapter 1, the FFLO state is a paradigm of exotic superfluidity. Realising and detecting the FFLO state has been long sought after and is one of the most important goals in our field. In Publication V we present a simple scheme for detecting the FFLO state by showing that the FFLO pairing momentum q is reflected in the time-of-flight expansion velocity of the edge of the gas cloud. The experimental realisation of our suggestion can be achieved in the set-up of [79] by turning off the trapping potential and measuring the density profiles as a function of time. Note however that our analysis assumes lattice, and the experiment by [79] is in continuum. We will address below how the lattice results should map to the continuum case.

Similarly as in Publications III and IV we employ TEBD with the Fermi-Hubbard Hamiltonian, this time with an infinite box potential which is the same for the both spin components (up and down). Initially we have a state with different number of up ($N_\uparrow$) and down ($N_\downarrow$) particles. As the FFLO is the ground state in 1D for any nonzero polarisation, we expect the ground state of the TEBD calculation to be a FFLO superfluid with pairing correlations n_k having a peak at the FFLO momentum q (see Equation 1.43). Then, we remove the trapping potential and examine the expansion dynamics of the system by looking at the density profiles $n_\uparrow$, $n_\downarrow$, and $n_{\uparrow\downarrow}$ obtained from the TEBD time evolution.

Figure 3.10 shows the ground state obtained from TEBD for $N_\uparrow = 10$, $N_\downarrow = 6$, and $\frac{U}{J} = -10.0$. Also the pairing correlation function n_k calculated using TEBD is shown. Indeed, we see that the system is a 1D FFLO superfluid, characterised by the peak at $q = k_{F\uparrow} - k_{F\downarrow}$ in n_k. Let us at this stage point out that we have experimented with systems with larger number of particles and larger lattices (up to $N_\uparrow = 0 - 40$, $N_\downarrow = 0 - 40$, $L = 320$ where L is the lattice size) and seen that the density profiles,

n_k as well as the subsequent dynamics remain similar and therefore it is sufficient to use lower particle numbers for which TEBD calculations are significantly less time consuming.

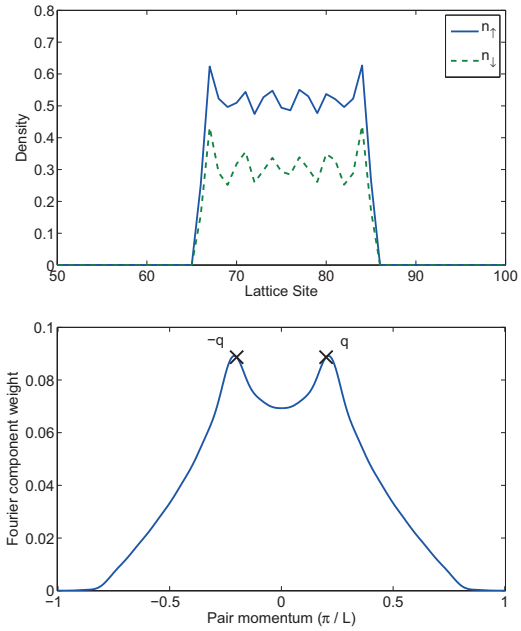

Figure 3.10. Above: The density profiles of up ($n_\uparrow$) and down spins ($n_\downarrow$) in the ground state when $N_\uparrow = 10$, $N_\downarrow = 6$, $\frac{U}{J} = -10$, and there is to a good approximation an infinitely strong repulsive potential everywhere except the at the lattice sites 66-85. Below: The pair momentum correlation function n_k for the same state. There are peaks at the FFLO momenta $q = \pm(k_{F\uparrow} - k_{F\downarrow}) = 0.2\pi/L$.

Figure 3.11 shows the doublon and unpaired particle density profiles after removing the trap as obtained from TEBD time evolution. The two-fluid picture discussed also in Publications III and IV is in place, as the pairs and unpaired particles expand ballistically just like non-interacting particles. Indeed, we have compared the expansion profiles of non-interacting profiles and seen that x doublons and y unpaired particles expand from the trap qualitatively just like x and y non-interacting particles. The comparison is presented in the supplementary material of Publication V.

However, unlike in the band insulator expansion the momentum distribution is not flat, but it reflects the underlying many-body physics. The two fluids expand with velocities that are given by $v_{un} = \frac{dE}{dk} = 2J\sin(k)$ and $v_{\uparrow\downarrow} = \frac{dE}{dk} = \frac{4J^2}{U}\sin(k)$. In Figure 3.11 we do not see a single velocity of expansion, but a spread of velocities, corresponding to the momentum

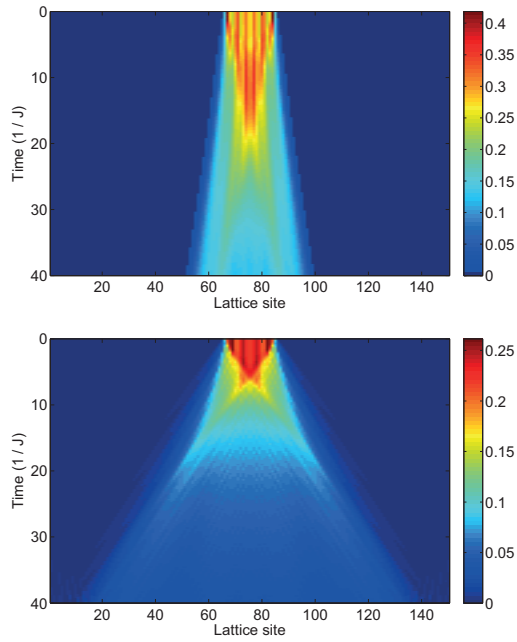

Figure 3.11. Above: The time development of the doublon density $n_{\uparrow\downarrow}(t)$. Below: The time development of the unpaired particle density $n_{\uparrow}(t) - n_{\uparrow\downarrow}(t)$.

distribution of the two fluids. The outermost expansion fronts for the doublons and unpaired particles reflect the maximum occupied momentum components of the two fluids. By measuring the speed of the expansion of the outermost wavefronts, the maximum occupied momenta are given by $k_{un}^{max} = \frac{1}{2J}\arcsin(v_{un}^{max})$ and $k_{\uparrow\downarrow}^{max} = \frac{U}{4J^2}\arcsin(v_{\uparrow\downarrow}^{max})$. Remarkably, we find that $k_{\uparrow\downarrow}^{max} = k_{F\downarrow}$ and $k_{un}^{max} = q$, where k_F denotes the Fermi momentum and q is the FFLO momentum. Therefore, by measuring the maximum expansion velocity of the unpaired component we obtain the FFLO momentum q from

$$q = \frac{1}{2J}\arcsin(v_{un}^{max}), \tag{3.18}$$

which is our main result. Measuring the maximum velocity from the expansion speed of the cloud edge[5] and comparing the result to the peak of n_k in the ground state we obtain the results presented in Figure 3.12. The results of Figure 3.12 show that the time-of-flight expansion provides us a

[5]The cloud edge corresponds to the highest occupied momentum component. In our simulations we see that the cloud edge expands with a constant velocity after the initial dynamics during which the highest occupied momentum component separates from the rest.

simple means for detecting the elusive FFLO state. It is noted that for the non-interacting case measuring the expansion velocity of the cloud edge gives $k_{F\uparrow}$ instead of q, and therefore the signature we see is genuinely caused by pairing, reflecting the FFLO peak in n_k.

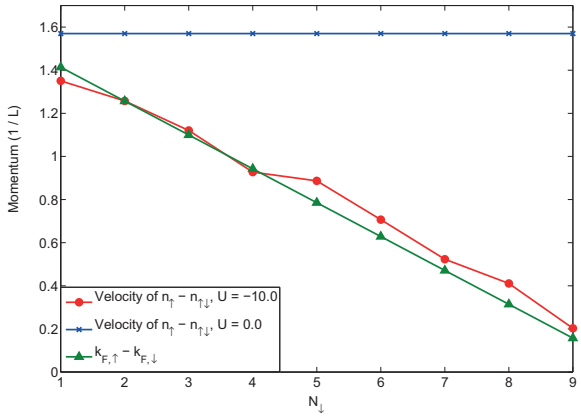

Figure 3.12. The FFLO momentum q determined from the edge expansion velocity of the unpaired cloud, compared to the q of the ground state, as a function of $N_\downarrow$ describing the imbalance ($N_\uparrow = 10$). We also show the expansion momentum $k \neq q$ obtained in the case of a non-interacting gas.

One would like to understand the physical origin of the observed momentum structure seen in our time-of-flight measurement. Comparing our results to the continuum Bethe Ansatz analysis for the Gaudin-Yang model [106] sheds light to the nature of the 1D FFLO state. In the Bethe Ansatz analysis in the strongly interacting limit it was found that the system separates into two families of solutions which can be identified as pairs and unpaired particles. These two fluids form separate Fermi seas, and the momentum structure is such that the highest populated momentum components are given by $k_{pair}^{max} = k_{F\downarrow}$ and $k_{un}^{max} = q$, in a perfect agreement with our numerical results in lattice. However, in the continuum model the dispersion relation of the unpaired particles is $k = \frac{k_{un}^2}{2m}$ (remembering $\hbar = 1$) and for pairs $k = \frac{k_{pair}^2}{4m}$. Thus in the strongly interacting Gaudin-Yang model the expansion velocity of pairs would not be suppressed like in the Fermi-Hubbard model with the on-site interaction U. Hence, in a continuum experiment pairs can actually expand with speeds comparable to unpaired particles, or even faster. Fortunately, in the current experiments [79] it is possible to resolve the hyperfine spin components separately and therefore measuring the maximum velocity of

the unpaired particles should not be a problem.

In Publication V we analysed also the case of harmonic trapping potential which is the form of trapping used in the experiments. The results shown in Figure 4b of Publication V are very similar to the results of the box trap.

Finishing the discussion on the results, let us briefly restate what we have discussed about detecting the FFLO state. We have suggested that the long-sought-for FFLO state can be detected in a time-of-flight measurement by measuring the expansion velocity of the unpaired particles. The detection could be achieved in the experimental setup of [79], keeping in mind the differences between the predictions of the continuum and lattice models.

References

[1] *Nobel Lectures, Physics 1971-1980*, Editor Stig Lundqvist, World Scientific Publishing Co. (1992).

[2] M.H. Anderson, J.R. Ensher, M.R. Matthews, C.E. Wieman, and E. Cornell, *Observation of Bose-Einstein condensation in a dilute atomic vapor*, Science **269**, 198 (1995).

[3] K.B. Davis, M.-O. Mewes, M.R. Andrews, N.J. van Druten, D.S. Durfee, D.M. Kurn, and W. Ketterle, *Bose-Einstein condensation in a gas of sodium atoms*, Phys. Rev. Lett. **75**, 3969 (1995).

[4] S.N. Bose, *Plancks gesetz und lichtquantenhypothese*, Z. Phys. **26**, 178 (1924).

[5] A. Einstein, *Quantentheorie des einatomigen idealen Gases: Zweite Abhandlung*, Sitzungber. Preuss. Akad. Wiss. **1925**, 3 (1925).

[6] The Nobel Foundation 9th September 2001 press release available at $http://www.nobelprize.org/nobel\_prizes/physics/laureates/2001/public.html$.

[7] J. Bardeen, L.N. Cooper, and J.R. Schrieffer, *Theory of superconductivity*, Phys. Rev. **108**, 1175 (1957).

[8] S. Jochim, M. Bartenstein, A. Altmeyer, G. Hendl, S. Riedl, C. Chin, J. Hecker Denschlag, and R. Grimm, *Bose-Einstein Condensation of Molecules*, Science **302**, 2101 (2003).

[9] M. Greiner, C.A. Regal, and D.S. Jin, *Emergence of a molecular Bose-Einstein condensate from a Fermi gas*, Nature **426**, 537 (2003).

[10] M.W. Zwierlein, C.A. Stan, C.H. Schunck, S.M.F. Raupach, S. Gupta, Z. Hadzibabic, and W. Ketterle, *Observation of Bose-Einstein Condensation of Molecules*, Phys. Rev. Lett. **91**, 250401 (2003).

[11] C.A. Regal, M. Greiner, and D.S. Jin, *Observation of resonance condensation of Fermionic atom pairs*, Phys. Rev. Lett. **92**, 040403 (2004).

[12] I. Bloch, J. Dalibard, and W. Zwerger, *Many-Body Physics with Ultracold Gases*, Rev. Mod. Phys. **80**, 885 (2008).

[13] S. Giorgini, L.P. Pitaevskii, S. Stringari, *Theory of ultracold Fermi gases*, Rev. Mod. Phys. **80**, 1215 (2008).

[14] W. Ketterle and M.W. Zwierlein, *Making, probing and understanding ultracold Fermi gases*, Proceedings of the International School of Physics "Enrico Fermi", Course CLXIV, Varenna, 20 - 30 June 2006, edited by M. Inguscio, W. Ketterle, and C. Salomon, IOS Press (2008).

[15] C. Chin, M. Bartenstein, A. Altmeyer, S. Riedl, S. Jochim, J. Hecker Denschlag, and R. Grimm, *Observation of the Pairing Gap in a Strongly Interacting Fermi Gas*, Science **305**, 1128 (2004).

[16] J. Kinnunen, M. Rodríguez, and P. Törmä, *Pairing Gap and In-Gap Excitations in Trapped Fermionic Superfluids*, Science **305**, 1131 (2004).

[17] M.W. Zwierlein, J.R. Abo-Shaeer, A. Schirotzek, C.H. Schunck, and W. Ketterle, *Vortices and Superfluidity in a Strongly Interacting Fermi Gas*, Nature **435**, 1047 (2005).

[18] W.S. Bakr, J.I. Gillen, A. Peng, S. Fölling, and M. Greiner, *A quantum gas microscope for detecting single atoms in a Hubbard-regime optical lattice*, Nature **462**, 74 (2009).

[19] N. Gemelke, X. Zhang, C.-L. Hung, and C. Chin, *In situ observation of incompressible Mott-insulating domains in ultracold atomic gases*, Nature **460**, 995 (2009).

[20] J.F. Sherson, C. Weitenberg, M. Endres, M. Cheneau, I. Bloch, and S. Kuhr, *Single-atom-resolved fluorescence imaging of an atomic Mott insulator*, Nature **467**, 68 (2010).

[21] J. Simon, W.S. Bakr, R. Ma, M.E. Tai, P.M. Preiss, and M. Greiner, *Quantum Simulation of Antiferromagnetic Spin Chains in an Optical Lattice*, Nature **472**, 307 (2011).

[22] H.F. Hess, *Evaporative cooling of magnetically trapped and compressed spin-polarized hydrogen*, Phys. Rev. B **34**, 3476 (1986).

[23] W. Ketterle and N.J. van Druten, *Evaporative cooling of trapped atoms*, Adv. At. Mol. Opt. Phys. **37**, 181 (1996).

[24] S. Kessler, A. Holzner, I.P. McCulloch, J. von Delft, and F. Marquardt, *Stroboscopic observation of quantum many-body dynamics*, in pre-print archive: http://arxiv.org/abs/1102.1605 (2011).

[25] Michael Tinkham, *Introduction to Superconductivity*, McGraw-Hill Book Co. (1975).

[26] U. Fano, *Effects of configuration interaction on intensities and phase shifts*, Phys. Rev. **124**, 1866 (1961).

[27] H. Feshbach, *A unified theory of nuclear reactions*, Ann. Phys. **19**, 287 (1962).

[28] T.B. Ottenstein, T. Lompe, M. Kohnen, A.N. Wenz, and S. Jochim, *Collisional stability of a three-component degenerate Fermi gas*, Phys. Rev. Lett. **101**, 203202 (2008).

[29] J.H. Huckans, J.R. Williams, E.L. Hazlett, R.W. Stites, and K.M. O'Hara, *Three-body recombination in a three-state Fermi gas with widely tunable interactions*, Phys. Rev. Lett. **102**, 165302 (2009).

[30] A.G.W. Modawi and A.J. Leggett, *Some properties of a spin-1 Fermi superfluid: Application to spin-polarized ^6Li*, J. Low Temp. Phys. **109**, 625 (1997).

[31] C. Honerkamp and W. Hofstetter, *Ultracold fermions and the SU(N) Hubbard model*, Phys. Rev. Lett. **92**, 170403 (2004).

[32] C. Honerkamp and W. Hofstetter, *BCS pairing in Fermi systems with N different hyperfine states*, Phys. Rev. B **70**, 094521 (2004).

[33] T. Paananen, J.-P. Martikainen, and P. Törmä, *Pairing in a three-component Fermi gas*, Phys. Rev. A **73**, 053606 (2006).

[34] L. He, M. Jin, and P. Zhuang, *Superfluidity in a three-flavor Fermi gas with SU(3) symmetry*, Phys. Rev. A **74**, 033604 (2006).

[35] R.W. Cherng, G. Refael, and E. Demler, *Superfluidity and magnetism in multicomponent ultracold fermions*, Phys. Rev. Lett. **99**, 130406 (2007).

[36] G. Catelani and E. A. Yuzbashyan, *Phase diagram, extended domain walls, and soft collective modes in a three-component fermionic superfluid*, Phys. Rev. A **78**, 033615 (2008).

[37] P. F. Bedaque and J. P. D'Incao, *Superfluid phases of the three-species fermion gas*, Ann. Phys. **324**, 1763 (2009).

[38] T. Ozawa and G. Baym, *Population imbalance and pairing in the BCS-BEC crossover of three-component ultracold fermions*, Phys. Rev. A **82**, 063615 (2010).

[39] O.H.T. Nummi, J.J. Kinnunen, and P. Törmä, *Coexistence of pairing gaps in three-component Fermi gases*, New J. Phys. **13**, 055013 (2011).

[40] F. Ferlaino, S. Knoop, and R. Grimm, *Ultracold Feshbach molecules*, Chapter in the book: "Cold Molecules: Theory, Experiment, Applications", edited by R.V. Krems, B. Friedrich and W.C. Stwalley, CRC Press (2009).

[41] C. Sanner, E.J. Su, W. Huang, A. Keshet, J. Gillen, and W. Ketterle, *Correlations and Pair Formation in a Repulsively Interacting Fermi Gas*, in pre-print archive: http://arxiv.org/abs/1108.2017 (2011).

[42] E. Tiesinga, B.J. Verhaar, and H.T.C. Stoof, *Threshold and resonance phenomena in ultracold ground-state collisions*, Phys. Rev. A **47**, 4114 (1993).

[43] H. Heiselberg, *Fermi systems with long scattering lengths*, Phys. Rev. A **63**, 043606 (2001).

[44] V. Gurarie and L. Radzihovsky, *Resonantly-paired fermionic superfluids*, Ann. Phys. **322**, 2 (2007).

[45] C. Chin, R. Grimm, P. Julienne, and E. Tiesinga, *Feshbach resonances in ultracold gases*, Rev. Mod. Phys. **82**, 1225 (2010).

[46] L. Radzihovsky and D.E. Sheehy, *Imbalanced Feshbach-resonant Fermi gases*, Rep. Prog. Phys. **73**, 076501 (2010).

[47] K.M. O'Hara, K.M. Hemmer, M.E. Gehm, S.R. Granade, and J.E. Thomas, *Observation of a strongly interacting degenerate Fermi gas of atoms*, Science **298**, 2179 (2002).

[48] K. Dieckmann, C.A. Stan, S. Gupta, Z. Hadzibabic, C. Schunck, and W. Ketterle, *Decay of an ultracold fermionic lithium gas near a Feshbach resonance*, Phys. Rev. Lett. **89**, 203201 (2002).

[49] T. Bourdel, J. Cubizolles, L. Khaykovich, K.M.F. Magalhães, S.J.J.M.F. Kokkelmans, G.V. Shlyapnikov, and C. Salomon, *Measurement of the interaction energy near a Feshbach resonance in a ^{6}Li Fermi gas*, Phys. Rev. Lett. **91**, 020402 (2003).

[50] C.A. Regal, M. Greiner, and D.S. Jin, *Lifetime of molecule-atom mixtures near a Feshbach resonance in 40K*, Phys. Rev. Lett. **92**, 083201 (2004).

[51] ALICE Collaboration: F. Carminati, P. Foka, P. Giubellino, A. Morsch, G. Paic, J.-P. Revol, K. Safarík, Y. Schutz, and U.A. Wiedemann (editors), *ALICE: Physics Performance Report, Volume I*, J. Phys. G: Nucl. Part. Phys. **30**, 1517 (2004).

[52] ALICE Collaboration, B. Alessandro, F. Antinori, J. A. Belikov, C. Blume, A. Dainese, P. Foka, P. Giubellino, B. Hippolyte, C. Kuhn, G. Martínez, M.Monteno, A. Morsch, T. K. Nayak, J. Nystrand, M. López Noriega, G. Paić, J. Pluta, L. Ramello, J-P Revol, K. Šafařík, J. Schukraft, Y. Schutz, E. Scomparin, R. Snellings, O. Villalobos Baillie, and E. Vercellin, *ALICE: Physics Performance Report, Volume II*, J. Phys. G: Nucl. Part. Phys. **32**, 1295 (2006).

[53] D.M. Eagles, *Possible pairing without superconductivity at low carrier concentrations in bulk and thin-film superconducting semiconductors*, Phys. Rev. **186**, 456 (1969).

[54] A.J. Leggett, *Diatomic molecules and Cooper pairs*, Modern Trends in the Theory of Condensed Matter, Proceedings of the XVIth Karpacz Winter School of Theoretical Physics, Karpacz, Poland, pp. 13–27, Springer-Verlag (1980).

[55] P. Nozières and S. Schmitt-Rink, *Bose condensation in an attractive fermion gas: from weak to strong coupling superconductivity*, J. Low Temp. Phys. **59**, 195 (1985).

[56] J. Carlson, S.-Y. Chang, V.R. Pandharipande, and K.E. Schmidt, *Superfluid Fermi Gases with Large Scattering Length*, Phys. Rev. Lett. **91**, 050401 (2003).

[57] G.E. Astrakharchik, J. Boronat, J. Casulleras, and S. Giorgini, *Equation of State of a Fermi Gas in the BEC-BCS Crossover: A Quantum Monte Carlo Study*, Phys. Rev. Lett. **93**, 200404 (2004).

[58] J. Carlson and S. Reddy, *Polarization Measurements and the Pairing Gap in the Universal Regime*, Phys. Rev. Lett. **100**, 150403 (2008).

[59] L. Tarruell, M. Teichmann, J. Mckeever, T. Bourdel, J.Cubizolles, L. Khaykovich, J. Zhang, N. Navon, F. Chevy, and C. Salomon, *Expansion of an ultra-cold lithium gas in the BEC-BCS crossover*, Proceedings of the International School of Physics "Enrico Fermi", Course CLXIV, Varenna, 20 - 30 June 2006, edited by M Inguscio, W Ketterle, and C Salomon, IOS Press (2008).

[60] J. Kinast, A. Turlapov, J.E. Thomas, Q.J. Chen, J. Stajic, and K. Levin, *Heat Capacity of a Strongly Interacting Fermi Gas*, Science **307**, 1296 (2005).

[61] G.B. Partridge, W. Li, R.I. Kamar, Y.A. Liao, and R.G. Hulet, *Pairing and Phase Separation in a Polarized Fermi Gas*, Science **311**, 503 (2006).

[62] M. Bartenstein, A. Altmeyer, S. Riedl, S. Jochim, C. Chin, J.H. Denschlag, and R. Grimm, *Crossover from a Molecular Bose-Einstein Condensate to a Degenerate Fermi Gas*, Phys. Rev. Lett. **92**, 120401 (2004); revised value M. Bartenstein, PhD. Thesis, Universität Innsbruck, (2005), p.100.

[63] J.T. Stewart, J.P. Gaebler, C.A. Regal, and D.S. Jin, *Potential Energy of a 40K Fermi Gas in the BCS-BEC Crossover*, Phys. Rev. Lett. **97**, 220406 (2006).

[64] P. Fulde and R.A. Ferrell, *Superconductivity in a strong spin-exchange field*, Phys. Rev. **135**, A550 (1964).

[65] A.I. Larkin and Y.N. Ovchinnikov, *Nonuniform state of superconductors*, Zh. Eksp. Teor. Fiz. **47**, 1136 (1964).

[66] H.A. Radovan, N.A. Fortune, T.P. Murphy, S.T. Hannahs, E.C. Palm, S.W. Tozer, and D. Hall, *Magnetic enhancement of superconductivity from electron spin domains*, Nature **425**, 51 (2003).

[67] A. Bianchi, R. Movshovich, C. Capan, P.G. Pagliuso, and J.L. Sarrao, *Possible Fulde-Ferrell-Larkin-Ovchinnikov Superconducting State in* $CeCoIn_5$, Phys. Rev. Lett. **91**, 187004 (2003).

[68] H. Won, K. Maki, S. Haas, N. Oeschler, F. Weickert, and P. Gegenwart, *Upper critical field and Fulde-Ferrell-Larkin-Ovchinnikov state in* $CeCoIn_5$, Phys. Rev. B **69**, 180504(R) (2004).

[69] T. Watanabe, Y. Kasahara, K. Izawa, T. Sakakibara, Y. Matsuda, C.J. van der Beek, T. Hanaguri, H. Shishido, R. Settai, and Y. Onuki, *High-field state of the flux-line lattice in the unconventional superconductor* $CeCoIn_5$, Phys. Rev. B **70**, 020506(R) (2004).

[70] C. Capan, A. Bianchi, R. Movshovich, A.D. Christianson, A. Malinowski, M.F. Hundley, A. Lacerda, P.G. Pagliuso, and J.L. Sarrao, *Anisotropy of thermal conductivity and possible signature of the Fulde-Ferrell-Larkin-Ovchinnikov state in* $CeCoIn_5$, Phys. Rev. B **70**, 134513 (2004).

[71] C. Martin, C.C. Agosta, S.W. Tozer, H.A. Radovan, E.C. Palm, T.P. Murphy, and J.L. Sarrao, *Evidence for the Fulde-Ferrell-Larkin-Ovchinnikov state in* $CeCoIn_5$ *from penetration depth measurements*, Phys. Rev. B **71**, 020503(R) (2005).

[72] K. Kakuyanagi, M. Saitoh, K. Kumagai, S. Takashima, M. Nohara, H. Takagi, and Y. Matsuda, *Texture in the Superconducting Order Parameter of* $CeCoIn_5$ *Revealed by Nuclear Magnetic Resonance*, Phys. Rev. Lett. **94**, 047602 (2005).

[73] S. Uji, T. Terashima, M. Nishimura, Y. Takahide, T. Konoike, K. Enomoto, H. Cui, H. Kobayashi, A. Kobayashi, H. Tanaka, M. Tokumoto, E.S. Choi,

T. Tokumoto, D. Graf, and J. S. Brooks, *Vortex Dynamics and the Fulde-Ferrell-Larkin-Ovchinnikov State in a Magnetic-Field-Induced Organic Superconductor*, Phys. Rev. Lett. **97**, 157001 (2006).

[74] K. Kumagai, M. Saitoh, T. Oyaizu, Y. Furukawa, S. Takashima, M. Nohara, H. Takagi, and Y. Matsuda, *Fulde-Ferrell-Larkin-Ovchinnikov State in a Perpendicular Field of Quasi-Two-Dimensional* $CeCoIn_5$, Phys. Rev. Lett. **97**, 227002 (2006).

[75] V.F. Correa, T.P. Murphy, C. Martin, K.M. Purcell, E.C. Palm, G.M. Schmiedeshoff, J.C. Cooley, and S.W. Tozer, *Magnetic-Field-Induced Lattice Anomaly inside the Superconducting State of* $CeCoIn_5$*: Anisotropic Evidence of the Possible Fulde-Ferrell-Larkin-Ovchinnikov State*, Phys. Rev. Lett. **98**, 087001 (2007).

[76] R. Lortz, Y. Wang, A. Demuer, P.H.M. Böttger, B. Bergk, G. Zwicknagl, Y. Nakazawa, and J. Wosnitza, *Calorimetric Evidence for a Fulde-Ferrell-Larkin-Ovchinnikov Superconducting State in the Layered Organic Superconductor* $\kappa-(BEDT-TTF)_2Cu(NCS)_2$, Phys. Rev. Lett. **99**, 187002 (2007).

[77] M. Kenzelmann, Th. Strässle, C. Niedermayer, M. Sigrist, B. Padmanabhan, M. Zolliker, A.D. Bianchi, R. Movshovich, E.D. Bauer, J.L. Sarrao, and J.D. Thompson, *Coupled Superconducting and Magnetic Order in* $CeCoIn_5$, Science **321**, 1652 (2008).

[78] W.A. Coniglio, L.E. Winter, K. Cho, C.C. Agosta, B. Fravel, and L.K. Montgomery, *Superconducting phase diagram and FFLO signature in* $\lambda-(BETS)_2GaCl_4$ *from rf penetration depth measurements*, Phys. Rev. B **83**, 224507 (2011).

[79] Y.-A. Liao, A.S.C. Rittner, T. Paprotta, W. Li, G.B. Partridge, R.G. Hulet, S.K. Baur, and E.J. Mueller, *Spin-imbalance in a one-dimensional Fermi gas*, Nature **467**, 567 (2010).

[80] T.K. Koponen, T. Paananen, J.-P. Martikainen, and P. Törmä, *Finite temperature phase diagram of a polarized Fermi gas in an optical lattice*, Phys. Rev. Lett. **99**, 120403 (2007).

[81] Y. Shin, C.H. Schunck, A. Schirotzek, and W. Ketterle, *Phase diagram for imbalanced fermionic superfluids: Phase diagram of a two-component Fermi gas with resonant interactions*, Nature **451**, 689 (2008).

[82] B.S. Chandrasekhar, *A note on the maximum critical field of high-field superconductors*, Appl. Phys. Lett. **1**, 7 (1962).

[83] A.M. Clogston, *Upper limit for the critical field in hard superconductors*, Phys. Rev. Lett. **9**, 266 (1962).

[84] T. Paananen, T.K. Koponen, P. Törmä, and J.-P. Martikainen, *Noise correlations of the ultracold Fermi gas in an optical lattice*, Phys. Rev. A **77**, 053602 (2008).

[85] A. Lüscher, R.M. Noack, and A.M. Läuchli, *Fulde-Ferrell-Larkin-Ovchinnikov state in the one-dimensional attractive Hubbard model and its fingerprint in spatial noise correlations*, Phys. Rev. A **78**, 013637 (2008).

[86] M.R. Bakhtiari, M.J. Leskinen, and P. Törmä, *Spectral signatures of the Fulde-Ferrell-Larkin-Ovchinnikov order parameter in one-dimensional optical lattices*, Phys. Rev. Lett. **101**, 120404 (2008).

[87] V. Gritsev, E. Demler, and A. Polkovnikov, *Interferometric probe of paired states*, Phys. Rev. A **78**, 063624 (2008).

[88] P. Kakashvili and C.J. Bolech, *Paired states in spin-imbalanced atomic Fermi gases in one dimension*, Phys. Rev. A **79**, 041603(R) (2009).

[89] J.M. Edge and N.R. Cooper, *Signature of the Fulde-Ferrell-Larkin- Ovchinnikov Phase in the Collective Modes of a Trapped Ultracold Fermi Gas*, Phys. Rev. Lett. **103**, 065301 (2009).

[90] Y.L. Loh and N. Trivedi, *Detecting the Elusive Larkin-Ovchinnikov Modulated Superfluid Phases for Imbalanced Fermi Gases in Optical Lattices*, Phys. Rev. Lett. **104**, 165302 (2010).

[91] J.M. Edge and N.R. Cooper, *Collective modes as a probe of imbalanced Fermi gases*, Phys. Rev. A **81**, 063606 (2010).

[92] A. Korolyuk, F. Massel, and P. Törmä, *Probing the Fulde-Ferrell-Larkin-Ovchinnikov Phase by Double Occupancy Modulation Spectroscopy*, Phys. Rev. Lett. **104**, 236402 (2010).

[93] M. Swanson, Y.L. Loh, and N. Trivedi, *Proposal for interferometric detection of topological defects in modulated superfluids*, in pre-print archive: http://arxiv.org/abs/1106.3908v1 (2011).

[94] I. Zapata, F. Sols, and E. Demler, *Triplet pair correlations in s-wave superfluids as a signature of the FFLO state*, in pre-print archive: http://arxiv.org/abs/1106.1605.

[95] Thierry Giamarchi, *Quantum Physics in One Dimension*, Oxford University Press (2004).

[96] F. Marsiglio, *Evaluation of the BCS approximation for the attractive Hubbard model in one dimension*, Phys. Rev. B **55**, 575 (1997).

[97] M.M. Parish, S.K. Baur, E.J. Mueller, and D.A. Huse, *Quasi-One- Dimensional Polarized Fermi Superfluids*, Phys. Rev. Lett. **99**, 250403 (2007).

[98] E. Zhao and W.V. Liu, *Theory of quasi-one-dimensional imbalanced Fermi gases*, Phys. Rev. A **78**, 063605 (2008).

[99] R. Casalbuoni and G. Nardulli, *Inhomogeneous superconductivity in condensed matter and QCD*, Rev. Mod. Phys. **76**, 263 (2004).

[100] H. Bethe, *Zur Theorie der Metalle Eigenwerte und Eigenfunktionen der linearen Atomkette*, Z. Phys. **71**, 205 (1931).

[101] E.H. Lieb and F.Y. Wu, *Absence of Mott Transition in an Exact Solution of the Short-Range, One-Band Model in One Dimension*, Phys. Rev. Lett. **20**, 1445 (1968).

[102] J. Y. Lee and X. W. Guan, *Asymptotic correlation functions and FFLO signature for the one-dimensional attractive spin-1/2 Fermi gas*, Nuclear Physics B **853**, 125 (2011).

[103] D.E. Sheehy and L. Radzihovsky, *BEC-BCS crossover in "magnetized" Feshbach-resonantly paired superfluids*, Phys. Rev. Lett. **96**, 060401 (2006).

[104] R. Combescot and C. Mora, *The low-temperature Fulde-Ferrell-Larkin-Ovchinnikov phases in 3 dimensions*, Europhys. Lett. **68**, 79 (2004).

[105] M.M. Parish, F.M. Marchetti, A. Lamacraft, and B.D. Simons, *Finite- temperature phase diagram of a polarized Fermi condensate*, Nature Physics **3**, 124 (2007).

[106] N. Oelkers, M. T. Batchelor, M. Bortz, and X. W. Guan, *Bethe Ansatz study of one-dimensional Bose and Fermi gases with periodic and hard wall boundary conditions*, J.Phys. A: Math.Gen. **39**, 1073 (2006).

[107] G. Vidal, *Efficient Classical Simulation of Slightly Entangled Quantum Computations*, Phys. Rev. Lett. **91**, 147902 (2003).

[108] J. Eisert, *Area laws for the entanglement entropy*, Rev. Mod. Phys. **82**, 277 (2010).

[109] S.R. White, *Density Matrix Formulation for Quantum Renormalization Groups*, Phys. Rev. Lett. **69**, 2863 (1992).

[110] U. Schollwöck, *The density-matrix renormalization group in the age of matrix product states*, Ann. Phys. **326**, 96 (2011).

[111] See e.g. Michael A. Nielsen and Isaac L. Chuang, *Quantum Computation and Quantum Information*, p. 109, Cambridge University Press (2000).

[112] Andrew Daley, *Manipulation and Simulation of Cold Atoms in Optical Lattices*, Dissertation zur Erlangung des akademischen Grades Doktor der Naturwissenschaften an der Fakultät für Mathematik, Informatik und Physik der Leopold-Franzens-Universität Innsbruck (2005).

[113] G. Baym and L.P. Kadanoff, *Conservation Laws and Correlation Functions*, Phys. Rev. **124**, 287 (1961).

[114] G. Baym, *Self-Consistent Approximations in Many-Body Systems*, Phys. Rev. **127**, 1391 (1962).

[115] Gerald D. Mahan, *Many-Particle Physics*, Kluwer Academic / Plenum publishers (1981).

[116] Z. Yu and G. Baym, *Spin-correlation functions in ultracold paired atomic-fermion systems: Sum rules, self-consistent approximations, and mean fields*, Phys. Rev. A **73**, 063601 (2006).

[117] M. Punk and W. Zwerger, *Theory of rf-Spectroscopy of Strongly Interacting Fermions*, Phys. Rev. Lett. **99**, 170404 (2007).

[118] S. Basu and E.J. Mueller, *Final-State Effects in the Radio Frequency Spectrum of Strongly Interacting Fermions*, Phys. Rev. Lett. **101**, 060405 (2008).

[119] Gh.-S. Paraoanu, M. Rodriguez, and P. Törmä, *Josephson effect in superfluid atomic Fermi-gases*, Phys. Rev. A **66**, 041603(R) (2002).

[120] F.H.L. Essler, H. Frahm, F. Göhmann, A. Klümper, and V.E. Korepin, *The One-Dimensional Hubbard Model*, Cambridge University Press (2005).

[121] U. Schneider, L. Hackermüller, J.P. Ronzheimer, S. Will, S. Braun, T. Best, I. Bloch, E. Demler, S. Mandt, D. Rasch, and A. Rosch, *Breakdown of diffusion: From collisional hydrodynamics to a continuous quantum walk in a homogeneous Hubbard model*, in pre-print archive: http://arxiv.org/abs/1005.3545.

[122] A. Sommer, M. Ku, G. Roati, and M.W. Zwierlein, *Universal spin transport in a strongly interacting Fermi gas*, Nature **472**, 201 (2011).

Because of their purity, controllability, and easy experimental access, fermionic quantum gases provide us an ideal playground for exploring condensed matter physics. With them one can study the physics behind interesting phenomena such as superfluidity and superconductivity. In the future, superconductors could be harnessed for energy-efficient transport of electricity. This thesis is a theoretical study of the physics of ultracold Fermi gases. We have used time-evolving block decimation algorithm (TEBD) and Kadanoff-Baym formalism to study both numerically and theoretically how the gases behave in different dynamical settings. The most important results presented within are the prediction of the existence of a spin-asymmetric Josephson effect, a theoretical picture explaining the dynamics of the Fermi - Hubbard model, and a suggestion for an easy way of detecting the long-sought-after Fulde-Ferrell-Larkin-Ovchinnikov (FFLO) superconducting state.

Aalto-DD 120/2011

ISBN 978-952-60-4372-2 (pdf)
ISBN 978-952-60-4371-5
ISSN-L 1799-4934
ISSN 1799-4942 (pdf)
ISSN 1799-4934

Aalto University
School of Science
Department of Applied Physics
www.aalto.fi